ESTABLISHMENT OF AN IN-SITU METHODOLOGY FOR WINDOW EVALUATION: CENTER OF GLASS U-VALUE

by

ABDULLAH J ALKHAMEES

B.SC., University of Colorado, Boulder, 2023

A thesis submitted to the

Faculty of the Graduate School of the

University of Colorado in partial fulfillment

of the requirement for the degree of

Master of Science

Department of Civil, Environmental and Architectural Engineering

2025

Committee Members:

Dr. Jay Arehart

Dr. John Zhai

Dr. Robert Tenent

Jennifer Scheib

Abstract

Alkhamees, Abdullah J (M.Sc., Architectural Engineering)

Establishment of An In-Situ Methodology for Window Evaluation: Center of Glass U-Value

Thesis directed by Professor Dr. John Zhai (Department of Civil, Environmental and Architectural Engineering)

Insulated Glass Units (IGUs) are often exposed to abnormal environmental conditions such as increasing global air temperatures applying physical stress to window components, leading to potential degradation in their energy performance. A methodology to compare the thermal transmittance of the IGUs provided by the window manufacturer to the U-value in-situ has not been established. A hybrid in-situ evaluation approach consisting of quantitative interior infrared (IR) thermography and the heat flux method (HFM) is proposed to estimate the average center of glass U-value by 6.2% in comparison to the computer-simulated COG U-value. The in-situ results are affected by the temperature gradient across the glazing system, as well as outdoor wind speed. Understanding the effects of longwave sky irradiance and assessing the methodology with a smaller temperature gradient can further ensure the robustness of this proposed methodology.

TABLES

FIGURES

CHAPTER I

INTRODUCTION

Beyond their traditional role as an opening for light penetration and natural ventilation, windows act as a dynamic envelope component that mediates heat transfer, daylight optimization, and thermal equilibrium within the built environment. The design, placement, orientation, angle of tilt and material composition directly influence the building's carbon footprint, indicating its transformative role in sustainable and energy-efficient architecture.

From an energy standpoint, windows enable passive solar heating and natural illumination, they can also represent thermal weak points in the building envelope. During the winter months, an inefficient window amplifies heat loss through convection and radiation, forcing the heating, ventilation and air conditioning (HVAC) equipment to compensate. Conversely, in the summer, excessive solar heat gained through inefficient windows can elevate indoor temperatures, increasing the building's cooling load [1]. The US Department of Energy estimates that windows account for 34% and 29% of annual HVAC energy consumption in commercial and residential buildings respectively [2]. These inefficiencies can stem from multiple factors, including improper installation of windows during construction, potential air leakage from the window cavity, inadequate insulation and poor solar heat gain coefficient (SHGC) ratings, all which can compound over a building's lifecycle.

The glazing system consists of three main components. The largest component of the window is the vision glass. It allows for the transmission of the largest amount of daylight into the building environment. Windows are classified as double or triple-pane based on the number of vision glass panes they contain, with double pane being the most installed window in the United States [3]. The vision glass paned are separated by the window cavity often contain a gas fill. These gas fills include and are not limited to krypton, xenon, argon and air. The vision glass panes and cavity configuration are sealed with the window frame, which is made from materials such as fiberglass, aluminum, wood. The National Fenestration Rating Council (NFRC) defines the energy rating of windows as the area-weighted average of the U-value (U_t) of each of the window components [4]. This is shown below as,

$$U_t = \frac{\Sigma A_{gv} U_{gv} + \Sigma A_f U_f + \omega}{A_t}$$

Thoughtful window selection is integral to energy-efficient building design, allowing for a pathway to optimize thermal performance, reduce annual building operational costs, and align with the global sustainability goals. Unlike simple glazing systems, more advanced window technologies can moderate the interplay between solar heat gain and visible light transmission. These innovations ranging from spectral selective coatings to multiple-pane configurations of vision glass with different gas fillers harness principles of material sciences to combine occupant comfort with energy conservation.

Low-emissivity (low-E) coatings, for instance, epitomize this balance between comfort and energy savings. By depositing microscopically thin metallic or ceramic layers onto glass surfaces, these selectively reflect mid and far-infrared radiation while maintaining high visible light transmittance. Some thin-film coatings are deposited using the RF magnetron sputtering technique and then laminated with transparent epoxy and polyvinyl butyral (PVB). Not only does this reduce unnecessary radiative heat transfer, but it further prevents the glass from shattering into small fragments when broken [5]. During the winter, internal heat is retained by reflecting heat back indoors, with solar radiation deflected outdoors due to the low-E coating. Apte et al. indicates that the use of low-emissivity windows in residential dwellings leads to 40% energy savings [2]. This highlights the role of windows as a step further towards building decarbonization. Emerging radiative cooling films further amplify this potential by combining spectral selectivity with passive heat mitigation. These films, often transparent or translucent, exhibit two complementary properties, high solar reflectance and high thermal emissivity. Studies on transparent radiative cooling films indicate potential annual air conditioning energy saving between 55.3%-63.4% [6].

The calculation of thermal transmittance (U-value) in opaque building components relies on a simplified one-dimensional heat flow model, where the heat transfer is assumed to be steady-state process like electrical current flowing through resistors in series. In this electro-thermal analogy, each homogenous material layer is assigned to a thermal resistance (R-value), analogous to an

electrical resistor, and the total U-value is derived by the summation of these resistances reciprocally.

$$U = \frac{1}{R_{tot}}$$

While this framework is mathematically correct, its practical accuracy hinges on idealized assumptions including uniform material properties and lateral heat flow, which these conditions are rarely met in real-world scenarios. For opaque building assemblies, such as walls or roofs, discrepancies between theoretical and in-situ U-values are well-documented. Studies report deviations ranging from +153% overestimation to -37% underestimation due to factors like thermal bridging, moisture infiltration and material degradation [7]. However, the challenge is amplified for fenestration systems where glass units introduce complexities not limited to multi-layer glazing and gas fillings. These create heterogenous thermal pathways that defy one-dimensional simplifications.

Compounding this issue creates a dynamic interaction between windows and their surroundings. Solar radiation, wind-driven convection, and temperature fluctuations alter heat flow in ways a controlled laboratory setting cannot replicate. Hot-box measurements, which allow U-value evaluation under controlled conditions, fail to consider potential window installation flaws such as improper sealing that vary window performance in-situ.

This gap between evaluation methods and empirical window performance is critical for fenestration, given their influence on building energy consumption.

Current evaluation methods lack robust in-situ validation tailored to fenestration systems. The establishment of such a methodology would require the utilization of present-day measurement techniques, including heat flux sensors and infrared thermography. Commercial windows have a life-span lower than that of their respective buildings at 50-60 years [1]. Without this, the building sector risks creating a cycle of inefficiency down the line, where optimized theoretical building models are underdelivered in practice, undermining both energy targets and stakeholder confidence.

Heat Flux Method

The heat flux method is a standardized in-situ evaluation method per ISO 9869 to determine the U-value of opaque building elements. It involves placing a heat flux sensor on the interior surface of the envelope element, in this context the window, and pairing it with temperature sensors on both the interior and exterior surfaces. Data is recorded over at least 72 hours assuming stable conditions. The U-value is calculated as the ratio of the average recorded heat flux over the average temperature difference.

The heat flux method is non-invasive, making it ideal for application in building elements, but would pose challenges with windows. These challenges are caused by the heterogenous nature of most new fenestration systems, which lead to underestimated or overestimated U-values. Out of 10 in-situ tests with theoretical U-values lower than 0.3 W/m2-k, only one resulted in an overestimated thermal

performance, with an average deviation of 0.2 W/m2-k. Overall, the measured U-value was 127% higher than theoretical values as shown in Figure 1 [8].

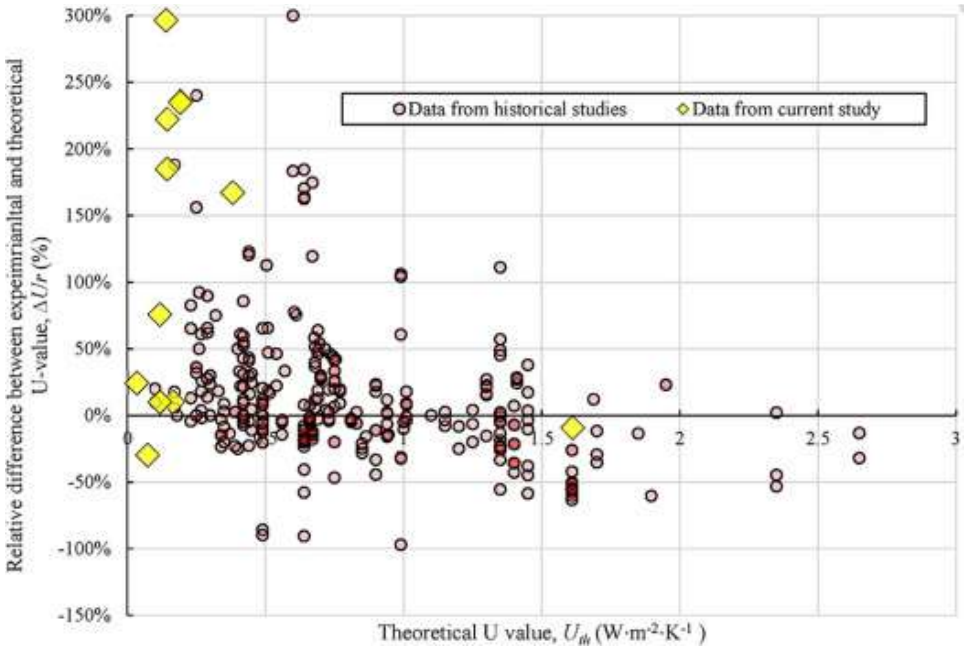

Figure 1: Comparison of theoretical U-values with the relative deviation of the experimentally measured U-value from and the theoretical value [8].

Such inconsistencies between both measured and theoretical values show how various factors such as variability of environmental conditions, solar radiation, could further exacerbate errors, necessitating more strict measurement protocols.

More strict measurement protocols are to be considered for windows, which tend to be more complex than their homogenous opaque envelope material counterparts [8].

Infrared Thermography

Infrared (IR) thermography is a non-destructive, non-contact method of measurement that captures temperature distributions across surfaces, enabling the detection of heat loss, thermal bridging, damage in thermal insulation, air leakage and condensation risk [9,10,11]. Unlike point-based methods such as heat flux meters, which provide localized, time-averaged data, IR thermography visualizes thermal anomalies across a larger surface area, offering a holistic view of a building material's thermal performance. The capability of IR thermography is advantageous for auditing building systems of different scales, from different HVAC systems to complex assemblies like windows [12]. This offers a holistic view of a building's thermal performance as well as windows, where heat transfer patterns are influenced by the frame, glazing layers and edge seals. By mapping surface temperatures, thermographers can identify patterns outside the visible light spectrum, which would hint at thermal inconsistencies within the system.

In comparison to heat flux meters, IR thermography significantly reduces inspection time while improving the spatial resolution of the window area assessed. On the other hand, the heat-flux method would require prolonged monitoring over 72 hours under a quasi-steady state. Given the shorter time frame, accurate U-value estimations through IR thermography demand controlled environmental parameters. Tejedor demonstrates that temperature differentials between indoor and outdoor environments critically influence accuracy. A temperature gradient of 7-16 °C during measurements introduced a 3.73% deviation between IR-derived U-

values and theoretical calculations across 583 thermograms [13]. To mitigate such errors, auditors must account for transient environmental factors such as solar radiation, wind speed, HVAC system schedule which alter surface temperatures independently from the window's physical properties.

Translucent materials, such as glass, pose unique challenges for IR thermography. These materials have partial transparency at certain infrared wavelengths, causing the camera to detect reflections from the surroundings. Compensating for reflected temperature is integral to avoid misinterpretation of the data, a process that requires calibration of the camera's emissivity settings and using auxiliary reference measurements [13]. Without these adjustments, reflections can compromise temperature readings, leading to uncertainties about thermal performance. These uncertainties are important to address as Nardi et al. shows that measured U-value had better estimations of thermal transmittance for lower reflected temperatures when the temperature difference increased [14].

CHAPTER II

LITERATURE REVIEW

Upon installation, the energy rating labels mounted on windows are removed [3]. The often-immediate removal of these labels emphasizes a gap in quality assurance after window installation and prior to occupancy. By visually inspecting glass, it is very difficult to identify window failures [3]. Without accessible thermal performance data, stakeholders cannot verify if windows meet manufacturer specifications after their installation. This necessitates the use of different measurement methods to ensure windows are performing as rated by the window manufacturer. The absence of such in-situ methodology fails to quantify any change in window performance over the building's lifetime if present.

The degradation of IGUs can be caused by both temperature and pressure fluctuations that affect the physical integrity of windows. Oxidation of glass sealants from ozone exposure further accelerates their deterioration [1]. These potential degradation pathways continue to show how fenestration systems can be thermal weak points in buildings, especially to abnormal environmental stressors. Over time, as global air temperatures continue to rise, thermal expansion can weaken window seals, further increasing physical and chemical degradation of the IGUs components. The complexity of window systems introduces multiple potential failure points which can degrade U-value performance. However, these defects can often remain undetected to the human eye until significant energy losses occur, emphasizing the need for proactive rather than reactive diagnostic tools. The use of infrared thermography has been used qualitatively in building audits. This shows

its useful application as well as its potential in quantitative analysis for thermal performance. With IR thermography, confidence in qualitative estimations could be low depending on the experience levels of the building auditor, failure to obtain sufficient boundary conditions of temperature difference for the identification of thermal bridges. Given that qualitative analysis is used to determine anomaly points in an object's surface, quantitative infrared thermography presents the extent of the defect as a number. The use of qualitative infrared thermography as a diagnostic tool helps identify defects that can then be quantified, allowing thermographers to assign numerical values to potential failures [11]. Researchers have been able to recognize that there are two problems associated with the use of IRT on glazing, those include the specular reflection of surrounding objects and inaccurate estimations of sky temperatures [15]. To tackle this, it is recommended that infrared images are taken from the inside of the space to reduce specular reflections. Furthermore, the use of a reference material of known emissivity eliminates the problem of reflection.

The potential for in-situ is possible with IGUs having a low thermal mass. Such low thermal mass induces a quasi-steady state condition that can be obtained under stable environmental conditions [15]. The approximation of thermal properties in windows is best conducted under conditions of significant temperature variation with minimal solar radiation. To achieve a quasi-steady state condition, it

would take 35-40 minutes after midnight, where solar radiation is zero, for windows as shown in Figure 2 below [16].

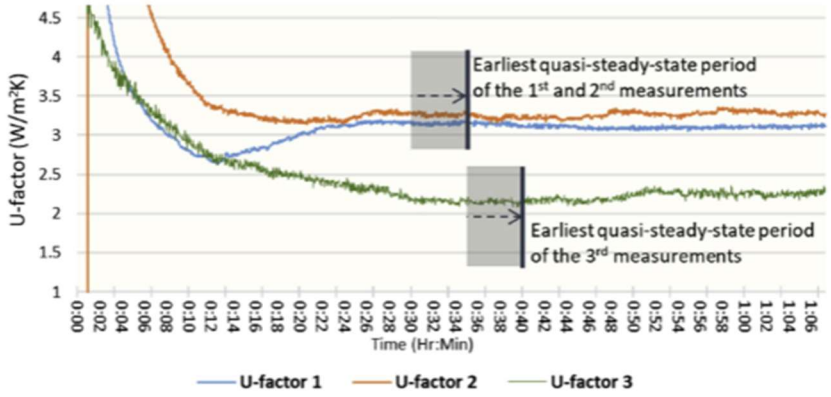

Figure 2: Every 5-min variation check [16].

The absence of solar irradiance eliminates direct solar heat gain caused by daylighting. This allows for a quasi-steady state to emerge. However, due to the specular reflectance of glass, it may result in infrared images that are not very reliable [15]. Overall, this gives the opportunity for in-situ window evaluation to be possible between 12:00 AM-6:00 PM, when sunlight is absent. Furthermore, the rapid ability for windows to equilibrate also heightens their sensitivity to residual heating or cooling during the night, necessitating precise timing to isolate the quasi-steady condition.

An inverse modeling approach was first developed by researchers to evaluate the energy performance of opaque building components. These estimations are often governed by:

- Historical data regarding material composition is often unreliable.

- Estimation based on preconstruction data to determine the theoretical U-value of the façade. These methods are standardized in ISO 6946 and can be obtained by building project managers.
- Estimation based on previous experimental data. [17]

To determine the minimum duration of in-situ HFM experiments, the consideration criteria were data quality, variability of results and the U-value for three walls based on ISO 9869 [17]:

- High U-value (2.35 W/m^2-k)
- Medium U-value (0.52 W/m^2-K)
- Low U-value (0.36 W/m^2-K)

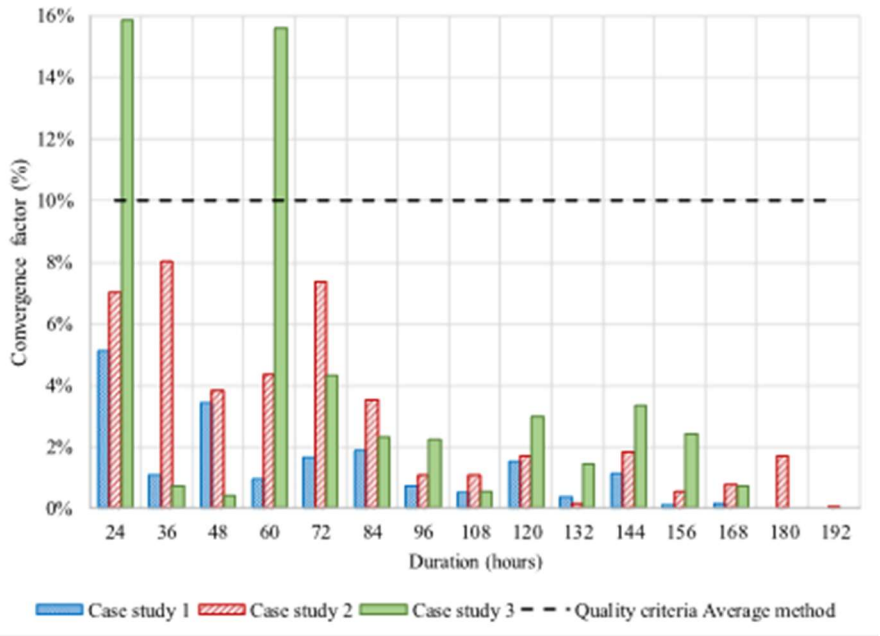

Figure 3: Data quality criteria in Case study 1, Case study 2, and Case study 3 using the average method [17].

The convergence factor of using the average heat flux method is presented in Figure 3, with high, medium and low U-value being case studies 1, 2 and 3 respectively. The convergence factor represents the difference between the determined U-value from experimentation and theoretical U-value. Walls with a low U-value have the highest convergence factor, necessitating the use of a longer duration time for testing. The results further indicate a variability of thermal transmittance values, with the largest swings in convergence factors between the 24–72-hour test duration. This highlights a critical consideration for in-situ window evaluations. Furthermore, actual windows and other building envelope components are exposed to dynamic environmental conditions, making the time-dependent reproducibility of results relatively low [11].

The difficulty in achieving time-dependent reproducibility is exacerbated by the lack of standardized methodologies for in-situ testing of windows. However, Choi provides a methodology for thermal bridges that improve confidence in a hybrid evaluation approach. This reflects the broader issue that without a rigorously defined methodology, reproducibility remains incomprehensible. To bridge the gap with a hybrid IRT-heat flux designed to alleviate convergence and reproducibility issues, synchronization of data from the different measurement devices is necessary to stabilize the results dynamically.

When it comes to IR thermography, it is necessary to induce quasi-steady state conditions with the measurement tools, which are done through installation of testing equipment 2-3 days before the infrared thermographs are taken. IR

thermography cameras require the identification of a region of interest, emissivity, reflected temperature and measurement angle [11]. The reflection of the IR camera, building auditor and incident angle can affect the accuracy of the results. However, the reflectance and emissivity of glass was determined to remain constant for incident angles under 45°. To eliminate the impact of systemic error on U-value measurements, it is suggested to gather as much information from the same instrument as possible [18]. This is driven by the difference accuracies of the measurement tools used in a hybrid testing approach.

A key component when dealing with convective and radiative heat transfer of surfaces is the determination of the object's emissivity. Avdelidis utilizes two different methodologies to determine the emissivity of different building materials. One approach utilizes the approach provided by ASTM E1933a and one where an empirical approach in a laboratory was used, using 3M Scotch Super 88 Vinyl tape. The materials were heated at 0 °C, 48.8 °C and 100 °C using a convection oven. From their experimentation, it was found that the emissivity of the materials varied based on the type of camera used. The most used IR cameras operate in mid-wavelength infrared (MWIR) and long-wavelength infrared (LWIR) which lie between 3-5 micrometers and 7-14 micrometers respectively. This is depicted in

Figure 4 where the variation in emissivity values at different temperatures vary with respective to the emissivity range that the cameras operate in [19].

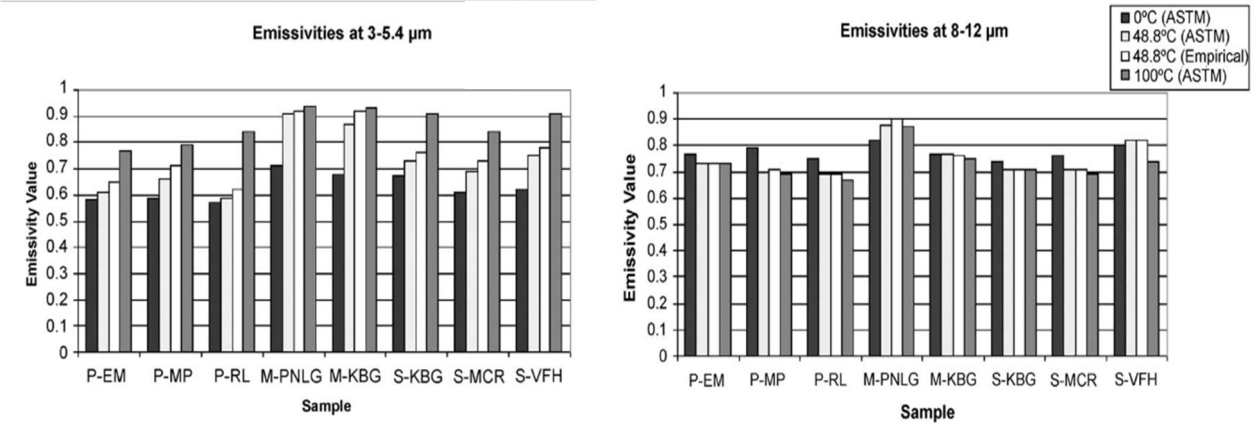

Figure 4: Emissivity values for materials in the 3-5.4 & 8-12 micrometer wavelength [19].

At the LWIR range, the measured emissivity values are more consistent across the different methodologies, indicating more precision in this wavelength. The absorption of radiation by these air particles is low in this range, which is supported by the increase in overall atmospheric transmittance at longer wavelengths [9].

The mean emissivity of windows determined in-situ was 0.85, with laboratory methods providing emissivity values ranging between 0.76 and 0.87 as shown in Figure 5 in Maroy's work [15,18].

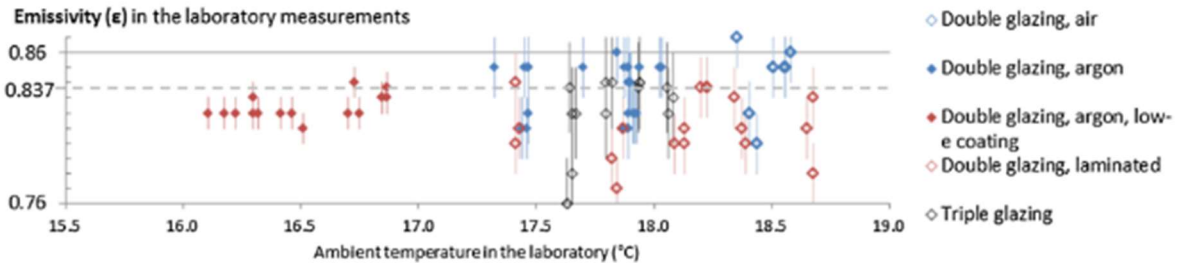

Figure 5: Window Emissivity Measured in the Laboratory with ASTM E1933-99a [18].

Maroy mentions that the ASTM 1993-99a method delivered variable emissivity values for the IGU's, which are thought to be caused by the specular reflectance effects in the laboratory. Understanding the effects of specular reflectance is not to be ignored as inaccuracies in U-value estimation are very sensitive. A deviation of 1 degree Celsius in the determination of the surface's reflective temperature could lead to a 10% error in the surface temperature. A 10% error in surface temperature translates to a 100% deviation in U-value.

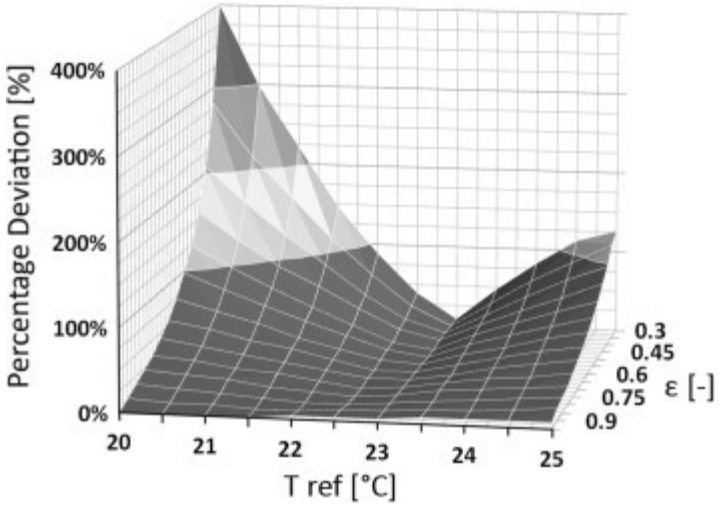

Figure 6: Percentage U-Value Calculation Sensitivity to Emissivity and Reflected Temperature [10].

Fokaides observes that during a 24-hour cycle, the reflected temperature of the indoor surface remains quasi-constant as it is very close to the ambient room temperature, whereas the outdoor reflected temperature of the same object experiences a larger temperature variation [10]. A change in the object's estimated emissivity value would affect radiative heat transfer due to its dependency on effectiveness in emitting radiative energy.

Internal infrared thermography is preferred over external methods due to its ability to mitigate environmental interference. Increases in surface temperature

due to solar radiation can reach 30 K or more. Without solar irradiation on non-opaque walls, the walls exhibited a –1 K deviation in surface temperature [20]. Wind, on the other hand, introduces challenges to the determination of the convective heat transfer coefficient, which amplifies thermal dispersion. Wind speeds higher than 5 m/s result can result in faulty IR thermography measurements [21]. These constraints complicate data accuracy and demand field conditions that are too ideal and impractical. By using internal infrared thermography, the variation caused by solar radiation and the measurement errors from fluctuating outdoor reflective temperatures are avoided. This dual advantage makes internal methods superior for precise U-value assessments.

While the heat flux method requires extending measurement periods for U-value calculations and is limited to localized measurement through a point on the window surface, infrared thermography offers rapid assessments under real-world conditions. IRT's ability to screen entire surfaces in an instant make it beneficial for building energy audits, and material evaluation including windows. Despite its limitations, infrared thermography remains a powerful detection tool for identifying thermal abnormalities. Combining these methods, auditors can bridge the gap between theoretical and empirical evaluations, leveraging the speed of IRT alongside the accuracy of the HFM under quasi-steady state conditions for thermal performance assessments.

CHAPTER III

EXISTING INDUSTRY STANDARDS

Accurate assessment of window performance requires rigorous application of existing standardized methodologies. Given the complex nature of fenestration systems, no single method is sufficient in capturing the full spectrum of the different heat transfer phenomena. The establishment of a hybrid approach in window performance evaluation is governed by standards:

- ASTM E1933a
- ISO 6781
- ISO 6946
- ISO 9869-1
- ISO 15099

The use of these standards provides the foundation for creating reliable and repeatable methods for the evaluation of windows. They dedicate the necessary protocols for data collection, stringent environmental control, and theoretical modeling. Together, they enable a holistic approach to diagnosing the thermal performance of windows.

ASTM E1933A

This standard is used to determine the emissivity of the window studied. It uses reference material with a known emissivity value, a reflective material in the form of a crumbled-up aluminum foil, and an infrared camera to determine the

emissivity of an unknown material [22]. The unknown material in this experimentation being the window assessed.

ISO 9869-1

This standard outlines the heat flux method for measuring in-situ thermal transmittance of building components. In steady state conditions, the standard defines the U-value as the quotient of the average heat flux over the average air temperature difference between the indoor and outdoor air where,

$$U_{avg} = \frac{q_{avg}}{T_{air,out} - T_{air,in}}$$

The average method was used where it mandates a monitoring period of no less than 72 hours under stable environmental conditions, with the use of heat flux sensors and temperature probes placed on both sides of the building element. The temperature difference between the interior and exterior environmental temperatures is to be 1-20 K. This standard assumes homogeneity of the opaque building material [23]. Given that ISO 9869 is limited to a point measurement, this necessitates the complementary data provided by IRT.

ISO 6781

This standard establishes guidelines for infrared thermography in building audits, highlighting the importance of controlled environments to ensure accuracy. It requires a minimum temperature difference of 10 °C between indoor and outdoor environments, low wind speeds and the avoidance of solar radiation during scans [24]. This allows for the IR camera to map surface temperature distributions

reliably. It allows for rapid identification of different zones of interest including the center of glass, edge and frame, where the heat flux sensors are to be placed. It further ensures that the recommended environmental conditions are met, which are required by ISO 9869 as well.

ISO 6946

The use of this standard governs the calculation methods used to determine the thermal transmittance in opaque building elements. ISO 6946 uses the electrical resistance analogy by summing up the thermal resistances in the multi-layer building element system [25]. Although this approach is effective for one-dimensional thermal analysis, it fails to account for the heterogenous nature of windows.

ISO 15099

This standard provides the in-depth calculations needed to determine the energy performance of windows in a laboratory setting. It provides the methodology for calculating the thermal transmittance of the window frame and vision glass, as well as the interaction of both [26]. This standard is adopted by the NFRC and LBNL establishing the national standard for window thermal transmittance as well as the WINDOW 7.8 energy simulation program that allows for simulation of center of glass thermal transmittance [27]. WINDOW 7.8 utilizes the IGDB that contains an array of different pieces of glass, both tested and verified by the NFRC.

CHAPTER IV

EQUIPMENT

In this experiment, multiple instruments were utilized to record temperature-related data with precision and reproducibility. Table 1 below represents the equipment used with their designated purpose. The infrared camera was placed on the tripod at a fixed distance of 1.0 meters away from the IGU. The tripod was extended to a height perpendicular to the surface-mounted heat flux meter and temperature sensor. The heat flux meter and temperature sensor were adhered to the center of the window surface using the highly reflective tape. The heat flux meter is connected to the FluxDAQ+ data acquisition tool, which connects the building's 120 Volts receptacle.

Table 1: Experimentation Equipment

Equipment	Model/Manufacturer	Key Specifications	Purpose
Infrared Camera	FLIR C5	Resolution: 160 x 120 (19,200 pixels) Accuracy: ±3 °C Spectral Range: 8 to 14 μm [28]	Window surface temperature mapping
Tripod	TONEOF 67" Cell Phone Selfie Stick Tripod	-	Tripod to stabilize infrared camera
Data Acquisition Tool	FluxTeq - FluxDAQ+ Data Logging System	Sensitivity: 1-2 W/m² [29]	Arduino-based acquisition tool used to record heat flux measurements

Heat Flux Sensor	FluxTeq – PHFS-01 Heat Flux Sensor	Sensitivity: 7.7 mV/(W/cm^2) Heat Flux Range: ± 150 kW/m^2 Temperature Range: -50 to +120 °C [30]	Records localized heat flux
Data Logger	Onset HOBO U12-012 Data Logger	Accuracy: ± 0.35 C from 0 to 50 °C, RH: ± 2.5% from 10% to 90% RH Operating Temperatures: -20 to 70 °C External Input Channel: ± 2 mV ± 2.5% of absolute reading [31]	Records indoor and outdoor surface and air temperature, and RH
TMCx-HE Temperature Sensor	Surface-mounted temperature sensor	Accuracy with U12: ± 0.25 C from 0 to 50 C Operating Temperatures: -40 to 100 C	Measures indoor and outdoor surface temperatures
High-emissivity tape	3M Scotch Vinyl Electrical Tape Super 88	Temperature Rating: -18 to 90 °C Color: Black [32] Emissivity: 0.95 [22]	Reference blackbody to calibrate camera
High-reflectivity tape	All Weather Aluminum Foil Tape	Temperature Rating: - 20 to 48 °C Color: Silver [33] Adhesive: Acrylic	• Used to mount HFM and temperature sensor on window surface • Used to determine window reflective temperature

Measuring Tape	Generic item	-	Used to measure window dimensions and distance.
GlassChek Elite	GC3200 - Glass Thickness Meter and Low-E Detector with Laminates	Glass Tolerance: ¼ in pane: 5.56-6.20 mm [34]	Identify glass pane thickness and low-E detector

Data Recording

The FluxDAQ+ tool, recordings heat flux and temperature readings from the indoor surface of the window every 3-4 seconds, whereas the HOBO data logger records relative humidity, luminous flux as well as surface and local air temperature. To allow for uninterrupted data acquisition over the 72 hour period, the HOBO data logger was set to recover temperature data every minute as shown in Figure 7 below.

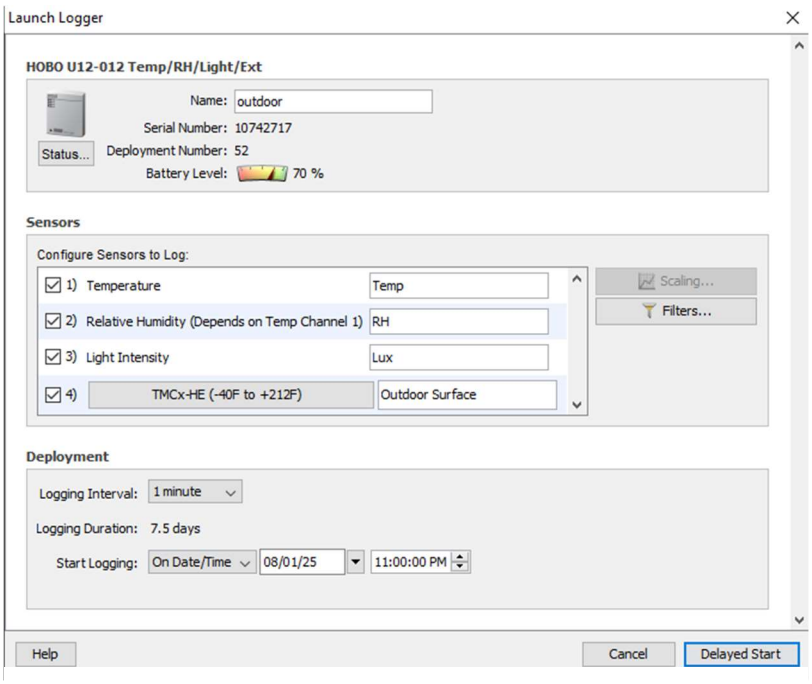

Figure 7: HOBO Data Logger Setup Window on HOBO Software

CHAPTER V

ESTABLISHING IN-SITU METHODOLOGY

The creation of the in-situ testing methodology was governed by the key findings from the literature review, where the interpration of data through percent difference, convergence factors between theoretical and tested U-value measurements, sensitivity of different measurements such as emissivity value, reflected temperature and wind speed were considered.

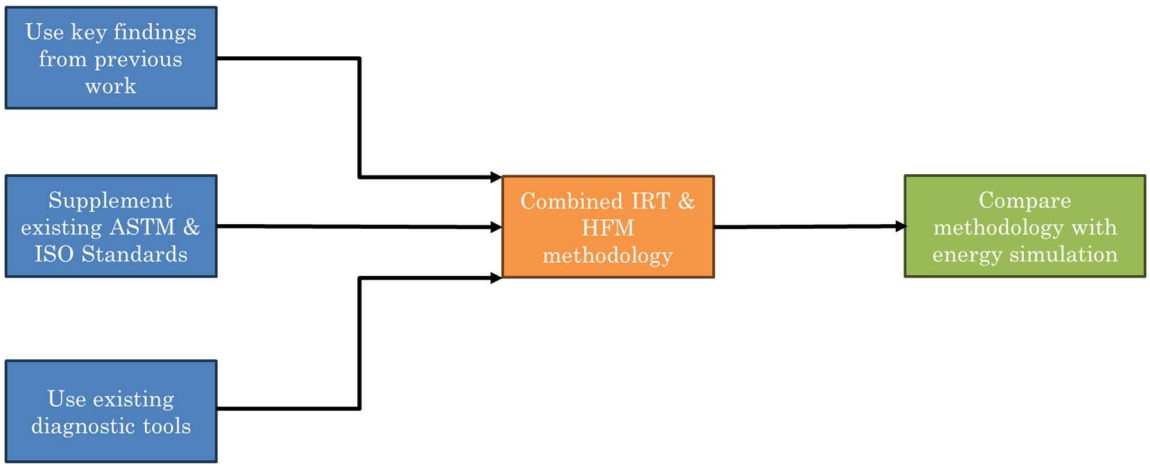

Figure 8: In-Situ Methodology Roadmap

As per Figure 8 above, the key findings from the literature review were carried forward to design the methodology for the in-situ test. Although it was understood that the time-reproducibility of the U-value estimations are challenging [11], the use of the heat flux meter required a testing period greater than 72 hours. Thus, temperature recordings were taken of the window surface were planned to take at least 72 hours or as long as the weather forecast permits where the wind speed is below 5 m/s [21]. The nocturnal measurements between 12:00-6:00 AM were taken based on Feng's findings [16]. The use of instantenous IR snapshots of the window

were used to determine the window's emissivity proteins. The ISO 9689-1 methodology was used to create one of the three comparisons needed to better understand the robustness of the proposed methodology. The proposed methodology under the name of "Simplified ISO 15099" methodology governed by assumptions following ISO 15099 were utilized to create the combined IRT and HFM methodology. After windows have been selected for testing, an initial field study was conducted to understand if ISO 9869-1 is applicable to windows was conducted.

Window Selection for Field Test

The preliminary phase of this research involved collecting window information provided by the operation and maintenance team on the building campus. The matrix of windows encompasses information such as glazing type, age, orientation. The quality of the information provided was ranked through a rating system based on:

- Level of detail: The availability of information regarding window geometry, design and material composition is integral to increase confidence in determined U-value from in-situ testing.
- Accessibility to building & testing location: Building remodeling and retrofitting is occurring at high volume on the campus being assessed, consideration of building accessibility. In-situ testing of windows is occurring in occupied buildings, thus spaces with low pedestrian foot traffic is necessary.
- Building walkthroughs: Testing site analysis through walkthroughs ensured proper coordination with building occupants and building maintenance team to allow for improved logistical coordination of in-situ testing. Educating building occupants adjacent to testing sites was necessary to avoid tampering with experimentation and verbal consent from the building occupants.

Initial Field Test

Following multiple site visits to assess candidate windows based on information provided, a service window of the campus cafeteria was selected due to its unobstructed access to a power outlet and its minimal surrounding interference including greenery and streetlamps from the outside and furniture from the indoors. The service window on the ground floor assessed is presented in Figure 9 below where exterior obstructions are minimal.

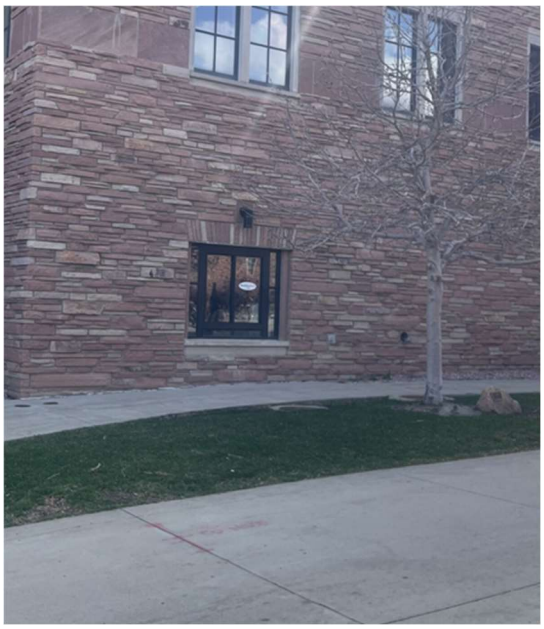

Figure 9: Initial Field Test window site

Importantly, the building's HVAC system was scheduled to shut down nightly between 11:00PM and 6:00AM, aligning with the proposed experimental time period. This inactive period ensured stable indoor air temperatures and eliminates the convective effects from the heating or cooling cycles, isolating the

conductive and radiative transfer mechanisms. These provide an ideal controlled environment for validating the heat flux methodology.

This window with a theoretical U-value of 1.59 W/m^2-K was selected to refine the heat flux method for fenestration system in-situ. Heat flux sensors were mounted on the interior center-of-glass surface using clear, double-sided tape. To ensure precise temperature measurements, the thermocouples were positioned adjacent to the heat flux sensor on both the interior and exterior window surfaces as shown in Figure 10.

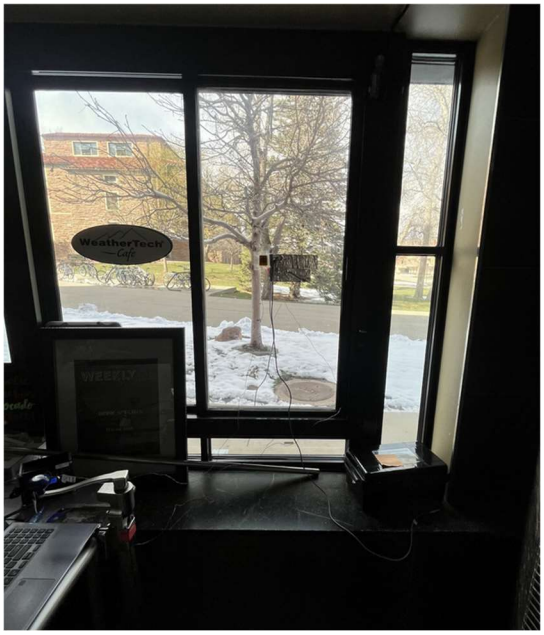

Figure 10: Heat Flux Sensor on the left with temperature sensor behind high-reflectivity tape on the right

Care was taken to isolate the thermocouple adhesive tape from the heat flux sensor's mounting tape, ensuring no overlap or physical contact that could create localized thermal bridging. The exterior and interior thermocouples were aligned at the same position on the window surface, guaranteeing that the recorded

temperatures correspond to an identical point across the glazing unit. This synchronization of the equipment enabling accurate temperature calculations driven by conductive heat transfer. The center-of-glass U-value was measured as mentioned in ISO 9869-1. The experimental results demonstrate a consistent decrease in thermal transmittance over the three nights as shown in Table X. The temperature decreased as the outdoor temperatures rose from an average of 6.0 C to 12.0 C. The corresponding heat flux decreases as well, reflecting a reduced heat loss.

Table 2: Initial Field Test – Average Data

	q_{avg} [W/m²]	T_{in} [°C]	T_{out} [°C]	$\Delta T_{air,avg}$ [°C]	U-Value [W/m²-K]
Night 1	-20.0	19.0	6.00	13.0	1.59
Night 2	-18.0	19.0	8.00	11.0	1.55
Night 3	-13.0	21.0	12.0	9.00	1.51
Average U-Value [W/m²-K]	**1.53 ± 0.0437**				
Actual U-Value [W/m²-K]	**1.59**				

These fluctuations suggest that temperature fluctuations in a dynamic, real-world environment play a critical role in having a quasi-steady state condition in U-factor accuracy.

Campus Field Test

Following the preliminary testing methodology, which informed us about the proposed framework, the proposed field test focused on a west-facing window in the campus cafeteria, it was selected due to its controlled environment and minimal interference as shown in Figures 11a and 11b below.

Figure 11a: In-situ field test site

Figure 11b: In-situ field test window from indoors

Like the initial field test, the HVAC system is turned off at night to limit convective airflow to induce a quasi-steady state internal environment. No furniture or obstructions near the window, with minimal vegetation and streetlamp interference from the outdoor environment. This setup ensured compliance with ISO 6781's requirement for low wind speeds Table 3 below presents the information regarding the window sample provided by the building's maintenance team.

Table 3: Window Details from Provided Project Information

Vision Glass	- LowE coated, clear insulating glass - Thickness of each glass pane: 6.0 mm - Outdoor glass pane: Heat-strengthened float glass - Indoor glass pane: Fully tempered float glass - Gas fill: Air - Low-e coating: Sputtered on second surface - Winter U-factor: 1.59 W/m^2-K maximum - Summer Daytime U-factor: 1.48 W/m^2-K maximum - SHGC: 0.27 maximum

The three main objectives to be met with the experimental design are:

1) Validation of quasi-steady state conditions
2) Data synchronization
3) Emissivity calibration

The validation of quasi-steady state conditions is to be met by minimizing convective effects by controlling the effects of wind when possible. From the initial setup, high reflectivity tape was used to adhere to the temperature probe onto the indoor and outdoor window surface. Using tape to tightly seal the probe can significantly reduce the effects of wind on temperature measurement by addressing convective heat loss and potential radiative interference. The wind accelerates convective cooling by compromising the thermal boundary layer around the probe, which can artificially lower its temperature reading. Simultaneously, the reflectivity of the tape minimizes radiative heat exchanges with the environment by

reflecting ambient infrared radiation rather than absorbing or emitting it. The dual ability of mitigating convective cooling and stabilizing radiation helps maintain a quasi-stable microclimate around the probe, isolating it from the transient effects of wind. As for reducing the effects on air temperature readings, the outdoor HOBO data logger was placed in a black weatherproof electrical box. Using the electrical box indoors was deemed unnecessary as the indoor environment lacks wind and direct solar radiation.

Data synchronization is critical for ensuring accurate data acquisition when combining infrared thermography and heat flux measurements. Spatial data synchronization refers to the alignment of measurement across different measurement tools. The FLIR C5 is placed on a tripod aimed to be directly perpendicular to the window at 1 meter. Furthermore, it is important to ensure the data aligns in time. Since IRT captures instantaneous snapshots while the HFM records continuous data, mismatched timing can skew the correlations between both measurement devices. To avoid this, multiple thermographs are taken during the same one-minute interval that the HOBO data logger is set on. For example, during the nighttime measurements, a thermograph at 5:07 AM is to align with the 1-minute average HFM data at 5:07 AM. The data synchronization is then optimized in post-processing. Proper synchronization ensures that localized U-value measurements are correlated correctly. Without it, edge effects, thermal bridging or transient behaviors may be misconstrued.

Simplified 15099 Methodology Procedure

The proposed methodology, utilizing both IRT and manual heat flux calculations, consists of the following workflow:

1. Identify window to be studied: Locate the window that is to be studied and request for information if available.
2. Check weather conditions prior to testing: A high nocturnal temperature (=<10 C) swing of outdoor air temperatures is preferred.
3. Turn HVAC equipment off prior to testing: This ensures that local indoor air temperatures are equivalent to the indoor air temperatures near the window. Attach heat flux sensor to data acquisition tool and attach surface temperature sensor on data logger.
4. Set the time interval for data logger to 1 minute time resolution.
5. Clean and disinfect window surface to remove any existing debris. Ensure external moisture from disinfectants is on window surface.
6. Place GlassChek on window surface to determine presence of low-emissivity coating, thickness of each vision glass pane and the window cavity.
7. Mount temperature and heat flux sensors to the center of the glass. Adhere to surface using reflective tape. Place outdoor data logger inside a weatherproof

box. Position the box close to the window while preventing potential pedestrian obstruction as shown in Figure 12 below.

Figure 12: Weatherproof Box with Temperature Sensor

8. During testing periods of 12:00 AM through 6:00 AM, perform instantaneous IR thermography prior to astronomical twilight during testing duration. Setup presented in Figure 13 below.

Figure 13: In-Situ Field Test Setup

CHAPTER VI

POST PROCESSING

Determining Emissivity

Following ASTM E1933a, the emissivity of the window can be determined. The reflected temperature of the test object, which determines the total radiative energy emitted by the object and its interaction with the atmosphere prior before that information is received by the infrared camera, is determined by taking the average temperature of the highlight reflective tape of the sample object. A sample calculation is performed for one of the thermograms taking during testing. The average temperature is determined by using the "AREA" function in the FLIR Ignite Software, allowing building auditors to determine the average temperature of a given area of interest. As shown in Figure 14 below, the AREA function was used on the reflective tape, where a reflective temperature of 18.6 Celsius was recorded.

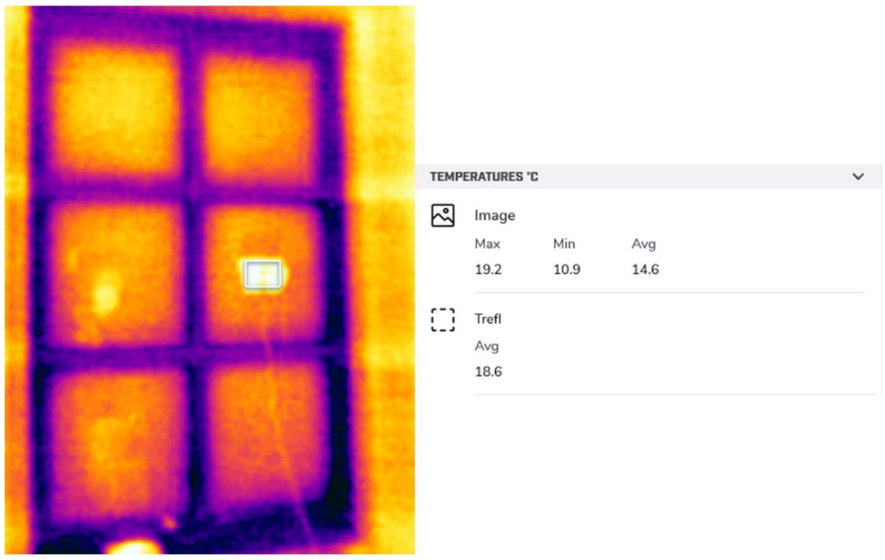

Figure 14: Reflected Temperature Determination Using FLIR Software

Within the FLIR software, the following parameters were input as shown in Figure 15.

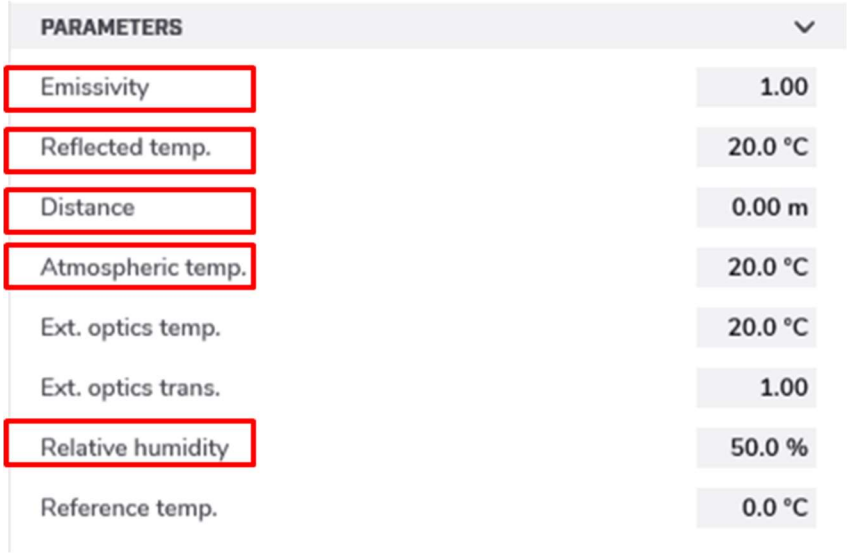

Figure 15: IR Camera Parameters

The instantaneous environmental data from the HOBO data logger including the indoor atmospheric temperature and relative humidity were inputted into each of the infrared snapshots taken by the FLIR C5 camera. The emissivity value of the sample object, the window, was then determined by varying the emissivity parameter of the infrared image taken until the temperature reading of the window is equal to the temperature reading of the reference object with known emissivity. The emissivity value of the reference object being the known emissivity value of ε_{ref} = 0.95. Using the AREA function once again, the emissivity value for the reference object was held at localized parameter constant at ε_{ref} = 0.95 as presented in Figure 16.

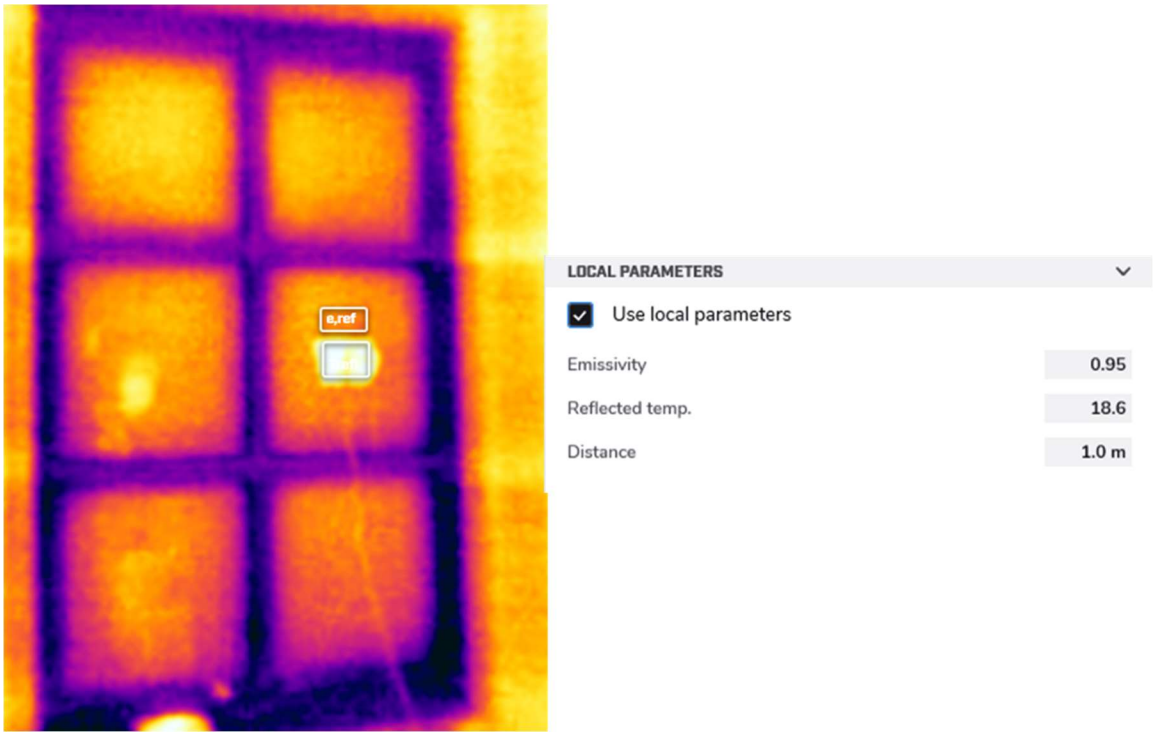

Figure 16: Localized Parameters for High Emissivity Tape

The average weighted average of the reference high-emissivity tape was determined to be 15.9 Celsius in this thermogram. After determining the necessary temperature values including the reflected temperature of the window and the temperature of the reference object, the emissivity of the window was determined by varying the emissivity parameter of the image presented area. Figure 17 below shows the AREA function utilized to determine the emissivity of the window. The rectangle used to determine the temperature of the reference object was copied with the FLIR Software. The rectangle in the software was positioned above the reference object measurement to massive spatial synchronization between both the reference temperature reading and the sample object. This creates a quasi-equivalency between both average temperature points, which allows for assumption

that both temperature readings are taken for points in space that are very close to each other to the window's center of glass.

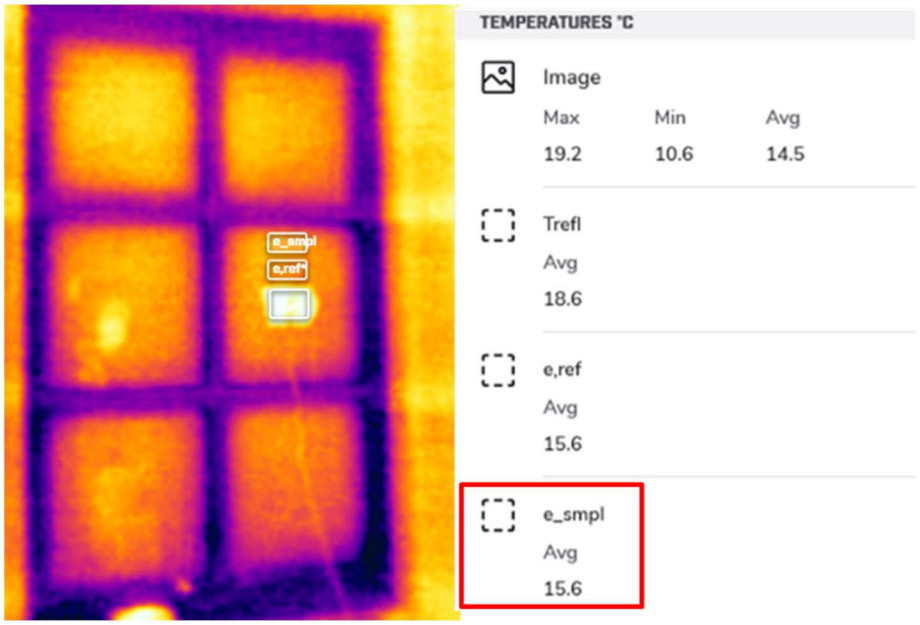

Figure 17: Window Temperature Determination using FLIR Software

Using ASTM E1933A, the emissivity of the window was determined to be 0.91. Utilizing this approach, the emissivity values extracted after calibrating the infrared images overestimates the emissivity of the window in a dynamic environment in comparison to Maroy's laboratory measurements, where the emissivity of the window was determined to be between 0.76 – 0.87 in ambient air temperatures of 15.5 °C and 19 °C [15]. To tackle this, a different emissivity calculation approach was used.

Revisiting the interaction between the target object, atmosphere and infrared camera was necessary. The FLIR C5, which is an LWIR thermal camera, was used due to its appropriate application for use with ambient temperatures [26]. Figure 18 considers the atmospheric transmittance values from National Aeronautics and

Space Administration's (NASA) ATRAN program with the LWIR that the FLIR C5 operates through [35]. As the wavelength increases, the atmospheric transmittance approaches 1.0 and then dips significantly after 13 micrometers.

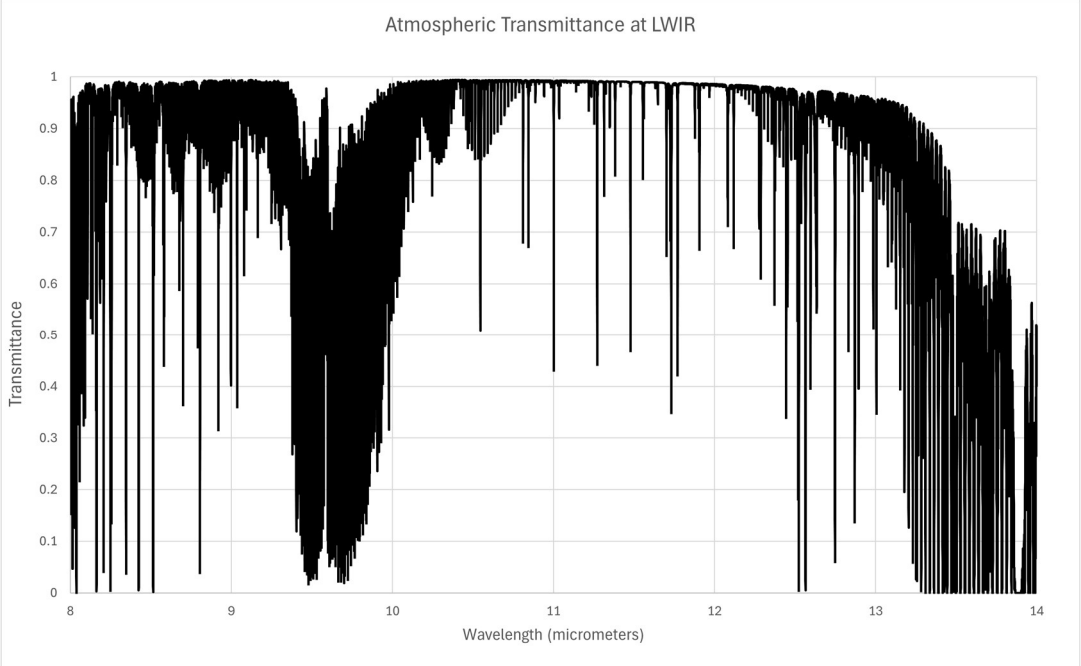

Figure 18: Atmospheric Transmittance at LWIR

The total radiant energy of the system is determined by the true temperature of the window specimen, which is denoted as the target object in Figure 19 [9].

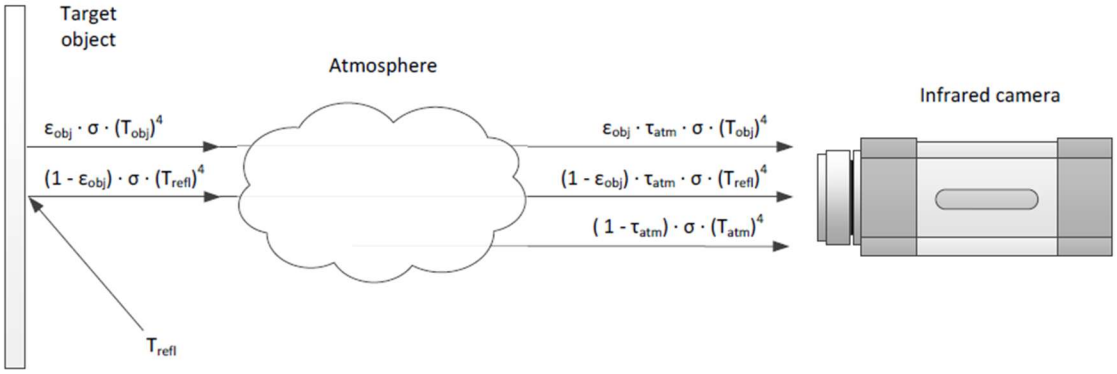

Figure 19: Interaction between infrared camera and target object [20].

The instantaneous temperature reading is determined by the thermocouple attached to the window specimen [9]. Therefore,

$$W_{tot} = E_{obj} + E_{refl} + E_{atm}$$

Given that,

$$W_{tot} = \sigma \cdot T_{e=1,window}^4$$

we get

$$\sigma \cdot T_{e=1,window}^4 = \epsilon_{obj} \cdot \tau_{atm} \cdot \sigma \cdot T_{obj}^4 + \left(1 - \epsilon_{obj}\right) \cdot \tau_{atm} \cdot \sigma \cdot T_{refl}^4 + (1 - \tau_{atm}) \cdot \sigma \cdot T_{atm}^4$$

Solving for ϵ_{obj}, which is the emissivity of the window, we get

$$\epsilon_{obj} = \frac{T_{e=1,window}^4 - \tau_{atm} \cdot T_{refl}^4 - (1 - \tau_{atm}) \cdot T_{atm}^4}{\tau_{atm} \cdot \left(T_{obj}^4 - T_{refl}^4\right)}$$

As shown above, the most important parameters are the specimen's apparent temperature, and reflected temperature, as highlighted by Choi [11]. The average temperature of the reflective tape, T_{refl} was taken from the FLIR Software. The

apparent temperature, $T_{e=1,window}$, takes the apparent surface temperature of the glass itself at a camera emissivity set to 1.0. The two temperatures recorded are carried forward along with the atmospheric temperature, T_{atm} from the data logger. T_{obj} is the object's surface temperature from the temperature sensor. These inputs are entered into the equation for ϵ_{obj} along with the constant τ_{atm}, which was taken based on the atmospheric transmittance values from the NASA ATRAN program, determining the emissivity of the window. The average ϵ_{obj} was determined to be 0.83, which aligns with the range of values presented in the literature view.

U-value Calculation

The center of glass U-value, U_{COG}, without solar radiation, is determined by the summation of individual resistance profiles of the different air conditions and surfaces per ISO 15099. The center-of-glass U-value considers interior and exterior heat transfer coefficients, the vision glass resistance, as well as the air cavity's heat transfer coefficient. Thus, the center-of-glass U-value is,

$$U_{COG} = \frac{1}{R_{tot}}$$

The two main heat transfer mechanisms that governed on interior and exterior surfaces are the combination of radiative and convective heat transfer. The convective and radiative heat on the internal surface, $q_{cv,int}$ and $q_{r,int}$ respectively are defined by ISO 15099 as,

$$q_{cv,in} = h_{cv,int}(T_{is} - T_{ia})$$

$$q_{r,in} = h_{r,int}(T_{is} - T_{ia})$$

where T_{is} is the indoor window surface temperature and T_{ia} is the indoor air temperature both in Kelvin [26]. For the combined radiative and convective heat transfer is defined as,

$$q_{comb} = h(T_s - T_a)$$

where T_s and T_a are the respective surface and air temperatures for the interior and exterior surfaces. The convective and radiative heat transfer coefficients on the exterior surfaces are defined as,

$$q_{cv,out} = h_{cv,out}(T_{os} - T_{oa})$$

$$q_{r,out} = h_{r,out}(T_{os} - T_{oa})$$

Calculation of External and Internal Heat Transfer Coefficient

As per Clause 8.3.3.2 and Clause 8.3.3.4 of ISO 15099, the calculation of the heat transfer coefficients on both the exterior boundary and interior boundary vary slightly, this is governed by the natural convection occurring in the indoor and forced convection occurring in the outdoor. ISO 15099 proposes two different methods to determine the outside convective heat transfer coefficient:

a) Product comparison rating
b) Real building (field situation) fenestration component [26]

Given the backwards modeling approach of the proposed methodology, the product rating approach is selected with the equation taken from ISO 6946,

$$h_{cv,out} = 4 + 4V_S$$

where V_S is the free stream velocity or localized wind speed in this case near the fenestration system in meters per second. The outdoor wind speeds at an elevation of 2 meters were retrieved from NASA's Prediction of Worldwide Energy Resources (POWER) project, which provides localized meteorologic data in an hourly time interval via the Modern-Era Retrospective analysis for Research and Applications, version 2 (MERRA-2) atmospheric reanalysis too [35-36]. The hourly wind speed parameters from the POWER project are used to quantify the average wind flow

around the region defined by the latitude and longitude of the experiment location with the exclusion of topography [37].

The interior heat transfer coefficient $h_{cv,int}$ is calculated based on the Nusselt number, Nu.

$$h_{cv,int} = Nu\left(\frac{\lambda_{ia}}{H}\right)$$

λ_{ia} is determined by a linear equation of coefficients from ISO 15099,

$$\lambda_{ia} = 0.002873 + 0.0000776T_{ia}$$

The height of the window is determined by the height of the vison glass analyzed, which is shown in Figure 20 below. H, is the height of the vision glass highlighted in red.

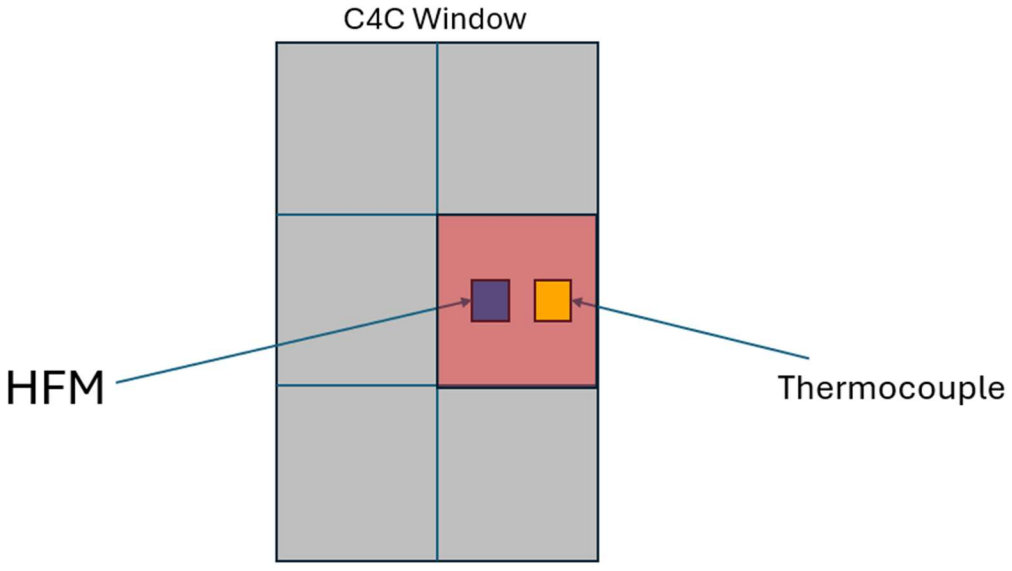

Figure 20: Equipment placement diagram

The Nusselt number is determined based on the corresponding Rayleigh, Ra, number which is another dimensionless number defined as,

$$Ra_H = \frac{\rho^2 H^3 g C_p |T_{is} - T_{ia}|}{T_{m,film} \mu \lambda}$$

$T_{m,film}$is the mean film temperature in Kelvin, which is defined as,

$$T_{m,film} = T_{ia} + 0.25(T_{is} - T_{ia})$$

Annex B of ISO 15099 determined the kinematic viscosity, specific heat, and thermal conductivity of air.

Given that the window is vertical and that the indoor air is warmer than the indoor surface the Nu is,

$$Nu = 0.13 Ra_H^{1/3}$$

The radiative heat transfer coefficients for the internal and external environments are then determined using the simplified radiative heat transfer calculation, where the radiative temperature near the surface is assumed to be equal to the air temperature recorded by the HOBO data logger. The internal and external surface emissivity values $\epsilon_{s,ext}$ and $\epsilon_{s,int}$ are replaced with the determined ε_{obj} in the equations for the radiative heat transfer coefficients [26],

$$h_{r,int} = \frac{\varepsilon_{s,int} \sigma (T_{is}^4 - T_{ia}^4)}{T_{is} - T_{ia}}$$

$$h_{r,ext} = \frac{\varepsilon_{s,ext} \sigma (T_{os}^4 - T_{oa}^4)}{T_{os} - T_{oa}}$$

The summation of the convective and radiative heat transfer coefficients provides us with the interior and exterior h values that can be used to determine the window's U-value, where [26],

$$h_{int} = h_{cv,int} + h_{r,int}$$

$$h_{ext} = h_{cv,ext} + h_{r,ext}$$

Calculation of Cavity Heat Transfer Coefficient

As per Clause 5 of ISO 15099, the simplified calculation of the convective heat transfer coefficient in the cavity, h_{cavity} is determined by calculating the cavity's Nusselt number, Nu_{cavity} [26],

$$h_{cavity} = Nu_{cavity} \frac{\lambda_{cavity}}{d_{cavity}}$$

To quantify the convective heat transfer coefficient, it is important to consider the angle of tilt of the IGU, which in this case is 90 degrees, thus the Nu_{cavity} is determined by the maximum of two small Rayleigh numbers, Ra_{cavity}.

$$Ra_{cavity} = \frac{\rho^2 H^3 g C_p |T_{is} - T_{ia}| \beta}{\mu \lambda}$$

ISO 15099 defines β as reciprocal of the cavity's mean temperature, and since that cannot be determined in a nondestructive manner, β_{cavity} is equal to [26]

$$\beta_{cavity} = \frac{1}{\frac{T_{is} + T_{os}}{2}}$$

The maximum of the two Nusselt numbers would be,

$$Nu_{cavity,1} = 1 + 1.7596 * 10^{-10} Ra_{cavity}^{2.2984755}$$

$$Nu_{cavity,2} = 0.242(\frac{Ra_{cavity}}{A_{gv,i}})^{0.272}$$

$A_{gv,i}$ is the aspect ratio of the air gap, which is equal to [26],

$$A_{gv,i} = \frac{H}{d_{cavity}}$$

The d_{cavity}, which is the thickness of the cavity, is retrieved from the Glass-Chek. The determination of the R_{gv} is governed by d_{glass} only. This is based on assumption that the thermal conductivity of the glass, which is unknown, is 1.0 W/m-K. Thus, the resistance of each glass pane is defined as the reciprocal of the glass thickness where,

$$R_{gv} = \frac{1}{d_{glass}}$$

This assumption is comparable to the thermal conductivity of the glass as defined by the WINDOW 7.8 simulation.

For the window analyzed, the Nusselt number in the cavity approaches 1.0, indicating that the convection and conduction forces in the gap are almost equal. This holds true for vertical windows as the correlation exists when there is no upper bound to the Rayleigh number and applies to cavities will low aspect ratios $A_{gv,i} <$ 25 as well [38].

By determining the convective heat transfer coefficients over the different boundaries, layers and cavities, the thermal resistance of the double-pane glazing system is

$$R_{tot} = \frac{1}{h_{ext}} + \sum R_{cavity} + \sum R_{gv} + \frac{1}{h_{int}}$$

Heat Flux Method

The COG U-value was calculated using the same approach in the initial field test where,

$$U_{COG} = \frac{q_{avg}}{\Delta T_{air,avg}}$$

The results from the heat flux method from ISO 9869-1 were used to compare the proposed simplified ISO 15099 method and WINDOW simulation discussed in Chapter 7.

CHAPTER VII

MODELING

To complement the empirical measurements, an inverse modeling approach was employed to simulate the thermal behavior of the window and deduce its characteristics. Simulating the experimental data allows for the identification of the overall structure of the insulated glass unit and cross-referencing it with the provided information from the building's maintenance department. The following outputs were carried forward to determine the characteristics of the window specimen:

- Indoor & Outdoor Air Temperatures
- Indoor & Outdoor Surface Temperatures
- Glazing system thickness
- Heat flux
- Calculated emissivity

WINDOW 7.8, a one-dimensional thermal analysis program by the Lawrence Berkeley National Lab (LBNL), was used to determine the characteristics of the glazing systems. The program contains the International Glazing Database (IGDB), an information repository published and maintained by the national lab. This database is used by organizations, such as the National Fenestration Rating Council & the US Department of Energy (DOE), to establish and support research regarding window rating systems.

The average indoor and outdoor air temperatures are used to create custom environmental conditions that match the environmental conditions of the in-situ measurements as shown in Table 4 below. The calculated h_{ext} and h_{int} were replaced by the default "Fixed combined coefficients" measurements are taken at night, the parameters regarding the SHGC are neglected. The wind speeds cannot be modified, the default V_S = 5.5 m/s was used for the simulation

Table 4: Environmental Parameters Inputted into WINDOW 7.8

	Environmental Conditions [°C]		Fixed Combined Coefficients [W/m²-K]	
Date	T_{oa}	T_{oa}	h_{int}	h_{ext}
Day 1	1.22	14.7	6.05	13.01
Day 2	2.25	15.1	6.07	18.34
Day 3	3.67	15.4	6.02	25.85
Day 4	8.12	16.5	6.03	12.70

Using the GlassChek diagnostics tool in-situ, information regarding the thickness of the glazing were carried forward to "Glazing Systems" to further identify the characteristics of the analyzed window. As shown in Figure 21, information regarding the window system was inputted into the program.

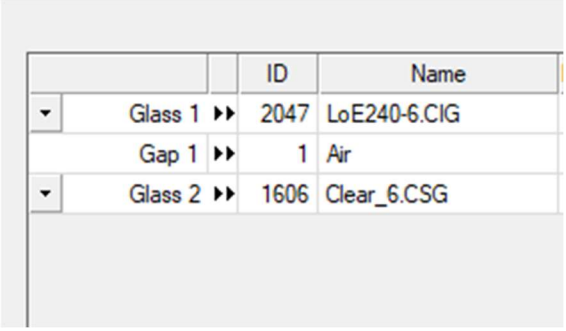

Figure 21: WINDOW 7.8 Glass Information

By varying the layers of "Glass 1" & "Glass 2", which are the outer and inner panes respectively, the existing glazing system can be predicted based on the center of glass U factor determined by the simulation. The simulated surface temperatures are then compared to the experimental surface temperatures to further determine the characteristics of the glazing system.

Steady State Simplification

Two panes and an air gap that are very thin. The thin gaps help explain the relationship between Nu and Ra, where Wright talks about the correlation used in earlier versions of WINDOW. Wright's new correlation explains the selection of the two Nusselt numbers proposed in ISO 15099. $Nu_{cavity,1}$ is based on Wright's correlation to vertical window cavities. $Nu_{cavity,2}$ is the previous work of ElSherbiny et al which shows the influence of Nu and Ra at low aspect ratios, $A_{gv,i}$. The correlations take the maximum of the two equations. To better understand how simplification holds true, a graphical comparison of the $Nu_{cavity,1}$ and $Nu_{cavity,2}$ at different aspect ratios are analyzed. Given that Wright's equation is only applicable

when Ra <= 10^4, the graphs below represent the concavity of both functions as the aspect ratio varies.

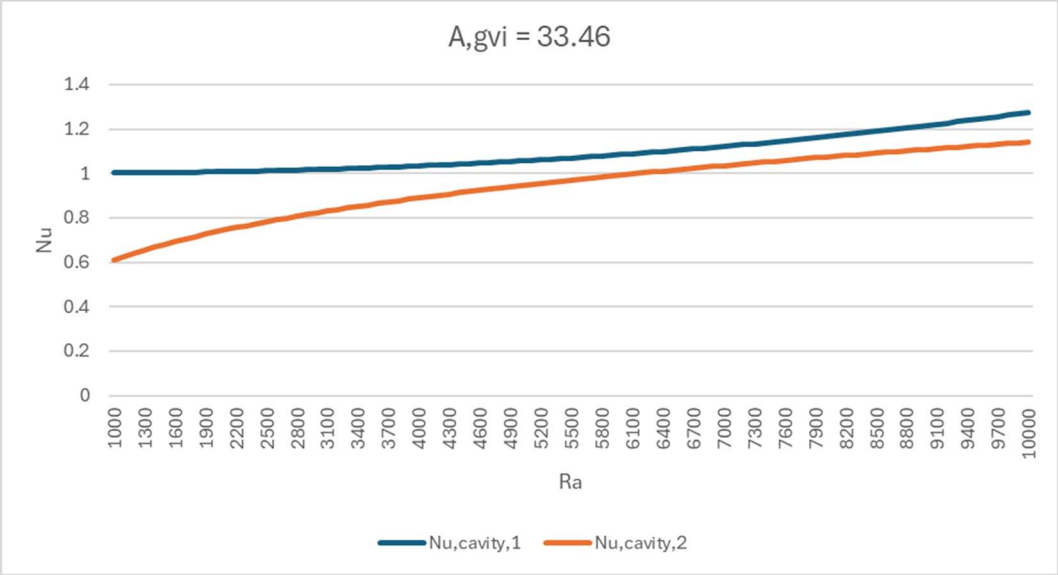

Figure 22: Nusselt number vs Rayleigh number of field test window and its aspect ratio.

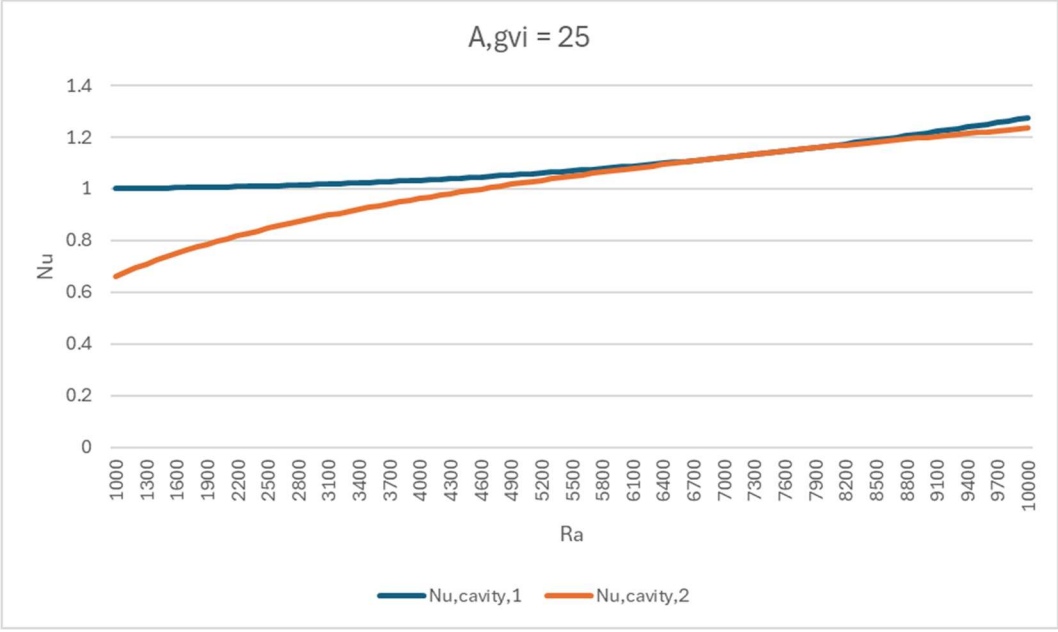

Figure 23: Nusselt number vs Rayleigh number of window with aspect ratio of 25.

Comparing the two Nusselt numbers at two different aspect ratios, $A_{gv,i}$ = 33.46 and $A_{gv,i}$ = 25, the Rayleigh number has a nonlinear dependence on both

equations. Up to Ra = 4500, $Nu_{cavity,1} > Nu_{cavity,2}$. This observation could lead to the conclusion that in relatively small vertical cavities, particularly in architectural windows, the convective and radiative heat flux are similar.

This simplification explains why the surface temperatures of the inner panes vary between WINDOW 7.8 and ISO 15099. The simplified approach only considers the inner and outer window surfaces. It does not consider the fact that each pane consists of a front and back temperature denoted as T_f and T_b respectively as shown in Figure 24 below [26].

For the non-vented case (5.3) the heat exchange by conduction/convection across a gap from one layer to the adjacent layer (pane, film or shading device) as given in 5.3.1: $q_{cv,i} = h_{cv,i}(T_{f,i} - T_{b,i+1})$, is split into two parts (see Figure 21), with the mean temperature of the air in the gap as a variable.

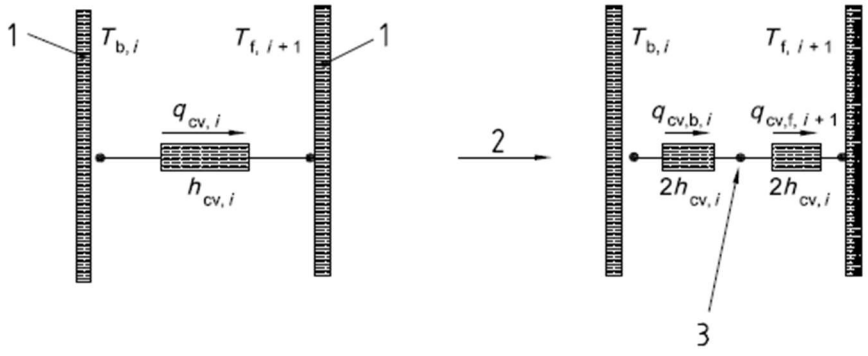

Key

1 pane or shading
2 split
3 $T_{gap,i}$

Figure 24: Cavity heat exchange for vertical windows [26]

This assumption underestimates the U-value, causing the magnitude of the COG U-value to be less than that from the simulation. The simplified methodology reduces the U-value calculation by 10%, which is driven by two factors, the low-

emissivity coating and the radiation effects. Figure 25 below translates Clause 7.4.2.2, where $T_{b,i}$ and $T_{f,i+1}$ are replaced with T_1, T_2, T_3, T_4.

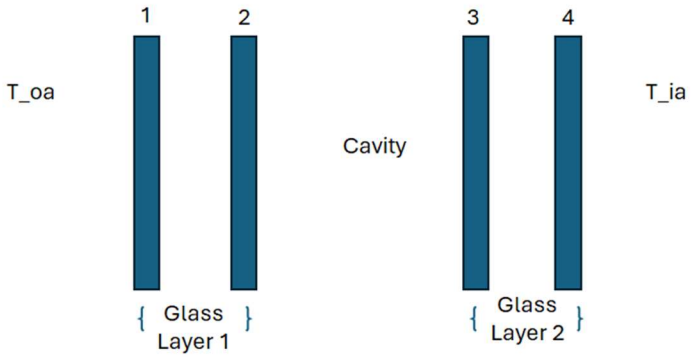

Figure 25: Double pane window diagram of assessed IGU

Each temperature corresponds to the absolute temperature of each surface. In the case of very small Nusselt numbers, where the convection and conduction forces are almost equivalent, the assumption that the radiative heat transfer and convective heat transfer within the air cavity are equivalent. By doing so, we can deduce the presence of the LowE coating as provided by the building maintenance team. The LowE coating was placed on surface 2 of the glazing system, therefore determine the emissivity of that coating. The emissivity of surfaces 1, 3 and 4 were assumed to be equal to ϵ_{obj} = 0.83. This becomes a radiative heat flux problem between two parallel vertical grey bodies that are separated by a distance of d_{cavity}. The solution to the following problem would be:

$$q_{rad,cavity} = \frac{\sigma(T_2^4 - T_3^4)}{\frac{1-\varepsilon_2}{\varepsilon_2} + \frac{1}{F_{2\to3}} + \frac{1-\varepsilon_3}{\varepsilon_3}}$$

$$\varepsilon_2 = \frac{1}{\frac{\sigma(T_2^4 - T_3^4)}{q_{rad,cavity}} - (\frac{1}{\varepsilon_3} - \frac{1}{F_{2\to3}})}$$

The view factor $F_{2\to3}$ is assumed to be 1 given the small distance of d_{cavity}. ε_3 is equal to ϵ_{obj}. This yields an emissivity value of ε_2 = 0.051. To ensure its correctness, it was compared to the emissivity values provided by the IGDB on WINDOW 7.8. Figure 26 shows that ε_2 = 0.051 conforms with the emissivity value of E2 for Glass 1, which follows the same numbering as Figure 25 above.

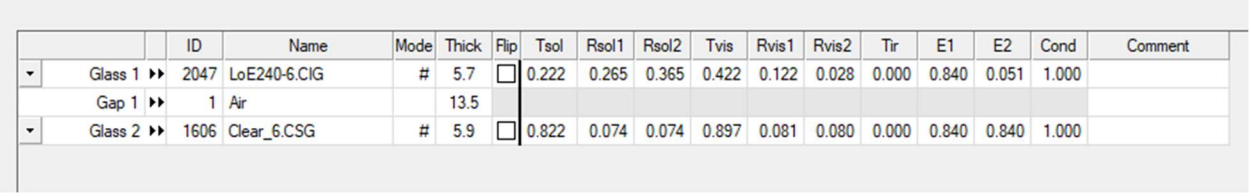

	ID	Name	Mode	Thick	Flip	Tsol	Rsol1	Rsol2	Tvis	Rvis1	Rvis2	Tir	E1	E2	Cond	Comment
Glass 1	2047	LoE240-6.CIG	#	5.7	☐	0.222	0.265	0.365	0.422	0.122	0.028	0.000	0.840	0.051	1.000	
Gap 1	1	Air		13.5												
Glass 2	1606	Clear_6.CSG	#	5.9	☐	0.822	0.074	0.074	0.897	0.081	0.080	0.000	0.840	0.840	1.000	

Figure 26: Glass layer details on WINDOW 7.8.

A comparison between the T_2 and T_3 the WINDOW 7.8 and simplified calculations are presented in Table 5 and 6 below,

Table 5: Simplified ISO 15099 Surface Temperature Results

Calculation Results [°C]						
		Glass Layer 1		Glass Layer 2		
	Outside Air	Outer Surface (T_1)	**Inner Surface** (T_2)	**Outer Surface** (T_3)	**Inner Surface** (T_4)	Indoor Air
Day 1	1.22	2.6	5.4	8.2	13.7	14.7
Day 2	2.25	3.3	6.0	8.7	14.1	15.1
Day 3	3.67	5.1	7.5	9.8	14.5	15.4
Day 4	8.12	9.3	10.9	12.5	15.7	16.5

Table 6: WINDOW 7.8 Surface Temperature Results

Window Results [°C]						
		Glass Layer 1		Glass Layer 2		
	Outside Air	Outer Surface (T_1)	**Inner Surface** (T_2)	**Outer Surface** (T_3)	**Inner Surface** (T_4)	Indoor Air
Day 1	1.22	2.6	2.7	11.5	11.6	14.7
Day 2	2.25	3.2	3.3	12	12.1	15.1
Day 3	3.67	4.2	4.3	12.5	12.6	15.4
Day 4	8.12	9.0	9.1	14.5	14.6	16.5

Chapter VII

DISCUSSION

Results

The results from the FluxDAQ+ using ISO 9869-1, the hybrid method established following ISO 15099, and the simulation results are in Table 7 and Figure 27 below,

Table 7: Summary of Results

Average COG U-Value [W/m2-K]						
Date	ΔT_{air} [K]	Average Wind Speed (m/s)	HFM only	ISO 15099	WINDOW 7.8	Simulation vs ISO 15099 Percent Difference
Day 1	13.5	1.28	1.25	1.29	1.37	**5.62%**
Day 2	12.9	2.61	1.24	1.33	1.42	**5.85%**
Day 3	11.8	4.47	1.18	1.36	1.47	**7.25%**
Day 4	8.40	1.13	1.00	1.29	1.38	**6.06%**

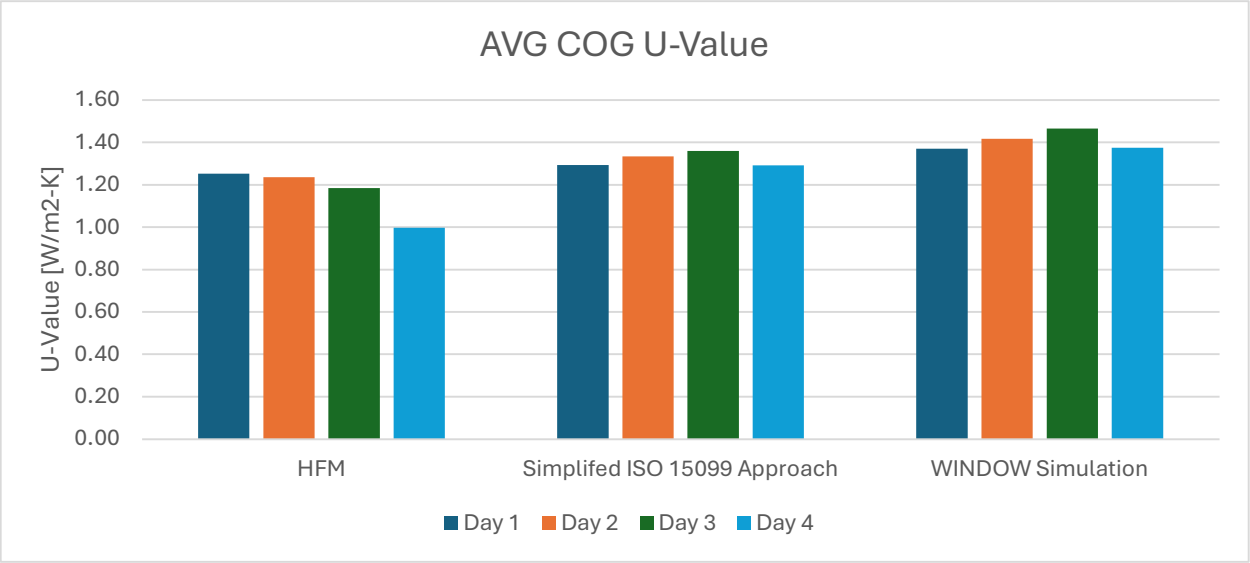

Figure 27: Average Center of Glass U-value Results

The variation in wind speed appeared to have an impact on the calculated results especially when comparing the average COG U-value over the different days

using the hybrid in-field approach using ISO 15099 and the simulation. The results for Day 3 show the highest U-value, indicating how the wind speed affects the outdoor convective heat transfer coefficient significantly. Looking at the equation for $h_{cv,out}$, a 1 m/s increase in wind speed, V_S, increasing $h_{cv,out}$ by 33%. Furthermore, a comparison between the different surface temperatures can be made that would allow for a better understanding of how the proposed methodology for COG U-value differs from the WINDOW 7.8 simulation which is based on ISO 15099.

Taking the average daily temperatures into WINDOW 7.8, allows the program to treat the parameters such as temperature, emissivity, and the different combined heat transfers coefficients as one point in time. This simplification makes the proposed methodology a one-dimensional steady state problem, which holds true in ISO 15099 in this context.

SENSITIVITY ANALYSIS

Collinearity of Outdoor Wind Speed & Temperature Difference

After compiling the results from the in-situ testing, further investigation of how the wind speed derived from NASA's MERRA-2 reanalysis and indoor-outdoor air temperature differences influence the calculated U-value. The goal is to identify whether wind and temperature differences act independently or codependently in the determination of in-situ thermal transmittance of windows.

The Variance Inflation Factor (VIF) is the tool used to measure the strength of multicollinearity between both environmental variables, wind speed and

temperature difference. A VIF of 1 indicates no multicollinearity, while values above 1 indicate the strength of the multicollinearity. The VIF_i for the environmental variables, i, is equal to

$$VIF_i = \frac{1}{1 - R_i^2}$$

where R is the coefficient of determination when the wind or temperature difference, ΔT, is regressed against the other. The VIF for each of the testing days were determined, along with the pooled data that aggregates the results while allowing for a broader perspective of the collinearity across the testing period as shown in Table 8.

Table 8: Variance Inflation Factor (VIF) of Environmental Conditions

	Wind Speed	Temperature Difference
Day 1	15.09	15.09
Day 2	2.1062	2.1062
Day 3	2.0091	2.0091
Day 4	1.2262	1.2262
Pooled Data	1.0446	1.0446

As shown in the first day, when taking the average hourly U-value with respect to the average wind speed from the MERRA-2 reanalysis tool, which approximates the regional wind speed very close to the testing site, an extreme collinearity exists where the VIF = 15.09. This indicates that on Day 1, the wind and temperature difference move together, which makes their individual effects inseparable. As for days 2-4, a lower collinearity exists, indicating a slightly lower codependency between both environmental factors and their influence on in-situ U-value calculations. Looking at Figure 28 below, when both outdoor wind speed and temperature difference is high, the U-value determined is higher.

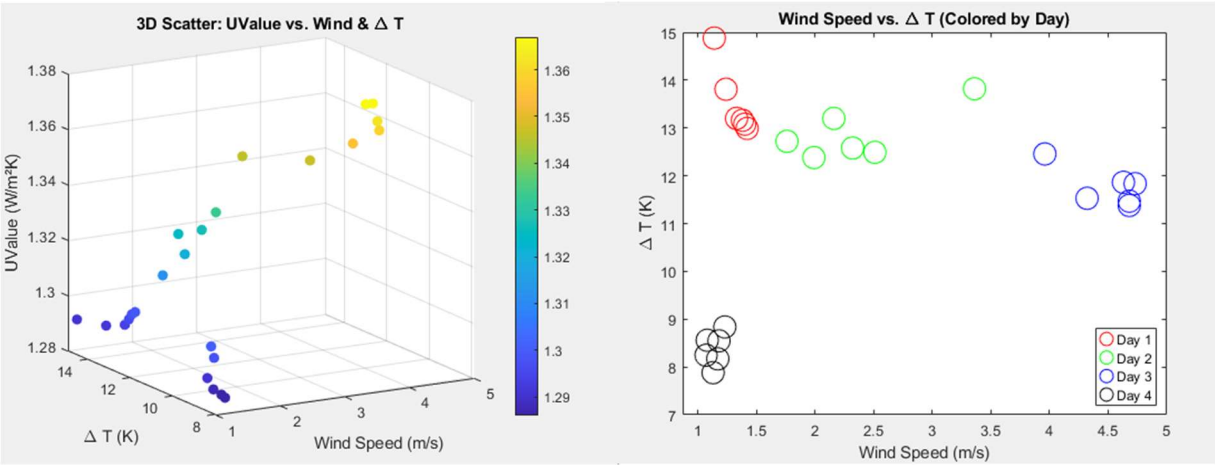

Figure 28: Relationship between temperature, wind speed and U-value

The same appears to be true when wind speed and temperature difference are both small where the U-value is lowest. This graphical representation of the different variables further presents a multicollinearity between wind speed and temperature difference. Looking at the variation in both wind speed and temperature difference in Figure 28, a larger variation is present on days 2-3, where both wind and temperature difference vary across a broad range of wind speed and

degrees Kelvin. The wind speed and temperature difference on Day 2 varies between 2.0-3.5 m/s and 12 K-14 K respectively.

A linear regression model was used to understand the effects of each of the respective environmental variables. Two forms of regression were considered, day-specific regression and aggregated regression modeling using the pooled data. The day-specific only considered the effects of both wind speed and temperature difference. For each testing day the regression equation is

$$U_{COG,daily} = \beta_0 + \beta_1 \cdot WindSpeed + \beta_2 \cdot \Delta T$$

where β_0 is the y-intercept when wind speed is 0 and ΔT is 0 K. β_1 is estimated coefficient for the change in U-value per 1 m/s wind increase when ΔT is 0 K. β_2 is the coefficient that takes into account the change in U-value per 1 K increase in temperature difference. As for the pooled data, it considers β_3, which addresses the effects of both wind speed and temperature difference on U-value.

$$U_{COG,pooled} = \beta_0 + \beta_1 \cdot WindSpeed + \beta_2 \cdot \Delta T + \beta_3 \cdot (WindSpeed \cdot \Delta T)$$

This interaction coefficient is omitted from the day-specific regression due to the smaller sample size. The daily models prioritize simplicity to isolate the effects of both wind and temperature difference, without including time-dependency. The da-day- specific linear regression modeling was conducted using the “fitlm” function in

MATLAB that fits the data using ordinary least squares (OLS) regression. The code used for the OLS regression is shown in Figure 29 below.

```
days = unique(data.Day);
for d = 1:length(days)
    day_data = data(data.Day == days(d), :);
    model_day = fitlm(day_data, 'UValue ~ WindSpeed + DeltaT');
    disp(['Day ', num2str(days(d)), ' Model:']);
    disp(model_day);
end
```

Figure 29: MATLAB Code for Linear Regression

For Day 1, where VIF is the highest, the day-specific linear regression model summary from MATLAB is presented in Table 9 below.

Table 9: Day-Specific Regression Model – Day 1

Coefficient	Estimated Value	Standard Error	T-Statistic	p-Value
β_0	1.146	0.035	33.168	0.000
β_1	0.061	0.010	5.823	0.010
β_2	0.005	0.002	3.248	0.048

The results of this day-specific linear regression allow us to understand the impact of each of the environmental factors. The magnitude of β_0 , which is 1.146 W/m^2-K serves as the U-value under a static environment where the temperature difference and outdoor wind speed are 273.15 K and 0 m/s respectively. This serves as the reference center of glass U-value for Day 1. For every 1 m/s increase in wind speed, the U-value increases by 0.061 W/m^{2}K. The +0.005 value for β_2 shows that for every 1 K increase in temperature difference, the U-value increases by 0.005 W/m^{2}K. The difference in their respective p-value explains their independent effects on the U-

value, with a higher statistical significance for the increase in wind speed on the overall U-value. Similar relationships are present on Days 2-4 when the VIF is lower in comparison to Day 1, where the effects of both temperature and wind are entangled depending on the testing conditions overall.

Aggregating the results allows for better understanding of the relationship between varying wind speed and temperature difference. With the pooled data's β_3 coefficient, it allows how an increase in wind speed and temperature difference both drive an increase in U-value, which is not observed in the day-specific regression models. From the literature review, it was found that wind does not impact U-value measurements, however the pooled data demonstrates otherwise. Table 10 below represents the interaction between wind speed and air temperature.

Table 10: Pooled Data Regression Model

Coefficient	Estimated Value	Standard Error	T-Statistic	p-Value
β_0	1.295	0.018	73.288	0.000
β_1	-0.006	0.013	-0.457	0.652
β_2	-0.002	0.002	-1.351	0.192
β_3	0.002	0.001	2.049	0.054

Prior studies often ignore the interaction between wind and temperature differences, while the pooled model shows that the both wind and temperature difference have a combined effect on the overall U-value across the aggregated testing data given the t-statistic value showing the association of both environmental variables on the U-value calculation. These findings challenge the oversimplified literature assumptions when dealing with wind effects on U-value

calculation, allowing the opportunity for improved in-situ testing protocols. Understanding wind and temperature differences would reduce the bias in the in-situ testing protocol, necessitating the measurement of wind speed very close to the testing site rather than the use of regional data.

Error Propagation

Understanding the effects of variable environmental conditions through the linear regression enhances external validity, which is heavily dependent on the dynamic nature of outdoor environment when performing the in-situ test. Prioritizing uncertainty based on the accuracy of measurement equipment further enhances the integrity of the simplified testing methodology proposed, which reduces bias in the raw data recorded from testing. The uncertainty of both the heat flux method and the simplified ISO 15099 methodology are heavily governed by accuracy of the infrared camera, data logger as well as the temperature sensor.

A root mean square method of error propagation was used for the heat flux methodology to understand its uncertainty which is governed by the heat flux sensor used, alongside the data logger and its temperature sensor. The heat flux method is governed by two variables, the temperature difference and the heat flux. The uncertainty of the heat flux method is defined as

$$\delta U_{glass,,avg} = \sqrt{(\frac{\delta q_{avg}}{q_{avg}})^2 + (\frac{\delta \Delta T_{air,avg}}{\Delta T_{air,avg}})^2}$$

where δq_{avg} is the dependent on the accuracy of the heat flux sensor, which is ±1-2 W/m², while $\delta \Delta T_{air,avg}$ is dependent on the accuracy of the data logger only of

±0.35°C. Table 11 below shows the standard uncertainty based on the error propagation for the heat flux method.

Table 11: Uncertainty of HFM

	Average COG U-Value (W/m²-K)
Day 1	1.25 ± 0.15
Day 2	1.24 ± 0.16
Day 3	1.18 ± 0.17
Day 4	1.00 ± 0.24

The uncertainty is heavily governed by the variation in temperature, where the error is amplified as determined by the literature review. The higher equipment error of the heat flux sensor of ±1-2 W/m² contributes more to the error in comparison to the data logger's accuracy when determining the U-value solely on heat flux.

As for the simplified approach utilizing both the infrared camera and the data logger. The uncertainty was determined based on the two pieces of equipment. To determine the total root-mean-square uncertainty from the emissivity, the statistical and equipment uncertainty, both $\delta\varepsilon_{obj,a}$ and $\delta\varepsilon_{obj,b}$ respectively. The statistical uncertainty $\delta\varepsilon_{obj,a}$ was determined based on the standard error of mean from $\varepsilon_{obj,n}$ from the n-th IR image uncertainty. The emissivity from the equipment, ε_{obj}, is defined as

$$\delta\varepsilon_{obj} = \sqrt{(\delta\varepsilon_{obj,a})^2 + (\delta\varepsilon_{obj,b})^2}$$

$$\delta\varepsilon_{obj,b}$$

$$= \sqrt{\left(\left(\frac{\partial\varepsilon_{obj}}{\partial T_{\varepsilon=1}}\right)\delta T_{\varepsilon=1}\right)^2 + \left(\left(\frac{\partial\varepsilon_{obj}}{\partial T_{refl}}\right)\delta T_{refl}\right)^2 + \left(\left(\frac{\partial\varepsilon_{obj}}{\partial T_{atm}}\right)\delta T_{atm}\right)^2 + \left(\left(\frac{\partial\varepsilon_{obj}}{\partial T_{obj}}\right)\delta T_{obj}\right)^2}$$

whereas. The average ε_{obj} of 0.83 from the five infrared images has an uncertainty of ± 0.0016. The emissivity value is carried forward into the simplified ISO 15099 methodology, where the uncertainty is defined as

$$\delta U_{COG} = \frac{\delta R_{tot}}{R_{tot}^2}$$

This error propagation is dependent on the different calculations completed in the simplified approach to determine the U-value uncertainty in each of the testing days. Table 12 below shows the uncertainty of the simplified, detailed approach which is less sensitive to changes in environmental temperatures due to its complexity.

Table 12: Simplified ISO 15099 Uncertainty

	Average COG U-Value (W/m²-K)
Day 1	1.29 ± 0.27
Day 2	1.33 ± 0.28
Day 3	1.36 ± 0.30
Day 4	1.29 ± 0.27

This is shown by the variation in the overall uncertainty during the testing days which ranges between ±0.27-0.30 W/m²-K. The use of the detailed approach gives us a better understanding of the environmental effects on the overall window

sample, allowing for more understanding how different components of the window system might change over time, especially when testing over a longer testing period.

CONCLUSION

U-value estimation of glass in a dynamic, real-world environment is extremely sensitive to environmental conditions, the calculation of the exterior convective heat transfer coefficient is heavily dependent on wind speed, necessitating the measurement of wind speed when estimating U-value. The use of a simplified approach to estimate the U-value of a given window has some promise as the change in average U-value over the 4 days is like the change in U-value with WINDOW 7.8. This similarity denotes the potential for this methodology to work with double-pane architectural windows with and without a low emissivity coating, especially with the average 6.2% deviation between the simplified calculation approach governed by ISO 15099 and the WINDOW 7.8 results.

To ensure the robustness of this methodology, it is integral to consider the effects of radiation amongst all the surfaces, taking into consideration sky coverage as well. This is highlighted through the difference in correlations between varying wind speeds and temperature differences. The simplified calculation further shows the accuracy of ISO 15099 when it comes to calculating the thermal transmittance of windows, which is why it is standardized and used in WINDOW 7.8.

The average COG U-value approach aligns with Gaspar's estimation approach where they consider the convergence of the calculated U-values over time.

However, such simplification fails to account for the transient effects throughout the night. The use of an IR camera that continuously records over time will allow for a better understanding and identification of thermal bridges and other potential anomalies with the glazing system. The duration of testing is inconclusive as the edge and frame effects haven't been accounted for yet.

Understanding the effects of both wind and temperature are integral for the center of glass U-value calculation given the center of glass is often the largest component in the window system. This is explained by the definition of thermal transmittance as presented by ISO and the NFRC. The use of anemometer whilst testing provides us with a larger sample size and better understanding of the overall transient effects of wind on U-value calculation. This would reduce uncertainty in sensitivity analysis, which would allow for a better understanding of the potential sources of error from utilizing this testing method. Improving the robustness of the testing method is the more informed building designers and building energy auditors can be when assessing the overall performance of different building materials including windows.

FUTURE WORK

Relative Humidity

The relationship between relative humidity (RH) and thermal conductivity introduces further complexities to in-situ U-value evaluation, more specifically with the heat flux method. As ISO 9689-1 assumes steady-state heat transfer under dry conditions, real-world relative humidity fluctuations, with a difference as small as

1%. Addressing these effects is key to further understanding the deviation between empirical and experimental U-values.

Hygroscopic materials such as window frames, insulation or degrading sealants can absorb moisture in high RH environments. Water molecules exhibit higher thermal conductivity than dry air, increasing their thermal conductivity. Condensation creates localized thermal bridges that further distort heat flux measurements. G. Ficco demonstrated that humidity-induced sensor drift can inflate U-value deviations in building materials [39].

The current center-of-glass methodology assumes minimal humidity impact on glazing and could underestimate edge-related heat transfer. To address this, future work will integrate the influence of relative humidity on edge location which would enable the development of a humidity-specific correction factor, reducing the discrepancies between theoretical and empirical window performance metrics.

Longwave Irradiance and Sky Temperature

Longwave irradiance from the atmosphere has impacts on heat loss of external surfaces of buildings. However, current regression models have only been able to yield annual CVRMSE (Coefficient of Variation Root Mean Square Error) value below 10% and not over shorter time periods [40]. The inclusion of sky irradiance with transient infrared thermography might allow for COG U-value testing using infrared thermography only.

Exterior Heat Transfer Coefficient

Improved refinement of the exterior heat transfer coefficient is necessary using anemometer to measure wind speed directly within the surroundings of the window assessed. This allows for better understanding of the effects of wind and temperature on the U-value calculation, further reducing uncertainty.

BIBLIOGRAPHY

[1] M. Likins-White, R. C. Tenent, and Z. (John) Zhai, "Degradation of Insulating Glass Units: Thermal Performance, Measurements and Energy Impacts," *Buildings*, vol. 13, no. 2, p. 551, Feb. 2023, doi: 10.3390/buildings13020551.

[2] J. Apte and D. Arasteh, "Window-Related Energy Consumption in the US Residential and Commercial Building Stock," LBNL--60146, 928762, Jun. 2006. doi: 10.2172/928762.

[3] K. Varshney, J. E. Rosa, and I. Shapiro, "Method to Diagnose Window Failures and Measure U-Factors on Site," *International Journal of Green Energy*, vol. 9, no. 3, pp. 280–296, Apr. 2012, doi: 10.1080/15435075.2011.641389.

[4] *ANSI/NFRC 100-2023: Procedure for Determining Fenestration Product U-factors*, Greenbelt, MD., 2023. [Online]. Available: www.nfrc.org

[5] M. Nur-E-Alam, M. Vasiliev, B. K. Yap, M. A. Islam, Y. Fouad, and T. S. Kiong, "Design, fabrication, and physical properties analysis of laminated Low-E coated glass for retrofit window solutions," *Energy and Buildings*, vol. 318, p. 114427, Sep. 2024, doi: 10.1016/j.enbuild.2024.114427.

[6] Z. Yi *et al.*, "Energy saving analysis of a transparent radiative cooling film for buildings with roof glazing," *Energy and Built Environment*, vol. 2, no. 2, pp. 214–222, Apr. 2021, doi: 10.1016/j.enbenv.2020.07.003.

[7] L. Evangelisti, C. Guattari, P. Gori, and R. Vollaro, "In Situ Thermal Transmittance Measurements for Investigating Differences between Wall Models and Actual Building Performance," *Sustainability*, vol. 7, no. 8, pp. 10388–10398, Aug. 2015, doi: 10.3390/su70810388.

[8] R. O'Hegarty, O. Kinnane, D. Lennon, and S. Colclough, "In-situ U-value monitoring of highly insulated building envelopes: Review and experimental investigation," *Energy and Buildings*, vol. 252, p. 111447, Dec. 2021, doi: 10.1016/j.enbuild.2021.111447.

[9] R. Usamentiaga, P. Venegas, J. Guerediaga, L. Vega, J. Molleda, and F. Bulnes, "Infrared Thermography for Temperature Measurement and Non-Destructive Testing," *Sensors*, vol. 14, no. 7, pp. 12305–12348, Jul. 2014, doi: 10.3390/s140712305.

[10] P. A. Fokaides and S. A. Kalogirou, "Application of infrared thermography for the determination of the overall heat transfer coefficient (U-Value) in building envelopes," *Applied Energy*, vol. 88, no. 12, pp. 4358–4365, Dec. 2011, doi: 10.1016/j.apenergy.2011.05.014.

[11] J.-S. Choi, C. Kim, H. Jang, and E.-J. Kim, "In-situ evaluation of window-wall joint performance using numerical models and thermal images," *Case Studies in Thermal Engineering*, vol. 45, p. 102988, May 2023, doi: 10.1016/j.csite.2023.102988.

[12] C. A. Balaras and A. A. Argiriou, "Infrared thermography for building diagnostics," *Energy and Buildings*, vol. 34, no. 2, pp. 171–183, Feb. 2002, doi: 10.1016/S0378-7788(01)00105-0.

[13] B. Tejedor, M. Casals, M. Gangolells, and X. Roca, "Quantitative internal infrared thermography for determining in-situ thermal behaviour of façades," *Energy and Buildings*, vol. 151, pp. 187–197, Sep. 2017, doi: 10.1016/j.enbuild.2017.06.040.

[14] I. Nardi, D. Paoletti, D. Ambrosini, T. De Rubeis, and S. Sfarra, "U-value assessment by infrared thermography: A comparison of different calculation methods in a Guarded Hot Box," *Energy and Buildings*, vol. 122, pp. 211–221, Jun. 2016, doi: 10.1016/j.enbuild.2016.04.017.

[15] K. Maroy, K. Carbonez, M. Steeman, and N. Van Den Bossche, "Assessing the thermal performance of insulating glass units with infrared thermography: Potential and limitations," *Energy and Buildings*, vol. 138, pp. 175–192, Mar. 2017, doi: 10.1016/j.enbuild.2016.10.054.

[16] Y. Feng, Q. Duan, J. Wang, and S. Baur, "Approximation of building window properties using in situ measurements," *Building and Environment*, vol. 169, p. 106590, Feb. 2020, doi: 10.1016/j.buildenv.2019.106590.

[17] K. Gaspar, M. Casals, and M. Gangolells, “Review of criteria for determining HFM minimum test duration,” *Energy and Buildings*, vol. 176, pp. 360–370, Oct. 2018, doi: 10.1016/j.enbuild.2018.07.049.

[18] M. Mahmoodzadeh, V. Gretka, K. Hay, C. Steele, and P. Mukhopadhyaya, “Determining overall heat transfer coefficient (U-Value) of wood-framed wall assemblies in Canada using external infrared thermography,” *Building and Environment*, vol. 199, p. 107897, Jul. 2021, doi: 10.1016/j.buildenv.2021.107897.

[19] N. P. Avdelidis and A. Moropoulou, “Emissivity considerations in building thermography,” *Energy and Buildings*, vol. 35, no. 7, pp. 663–667, Aug. 2003, doi: 10.1016/S0378-7788(02)00210-4.

[20] B. Lehmann, K. Ghazi Wakili, Th. Frank, B. Vera Collado, and Ch. Tanner, “Effects of individual climatic parameters on the infrared thermography of buildings,” *Applied Energy*, vol. 110, pp. 29–43, Oct. 2013, doi: 10.1016/j.apenergy.2013.03.066.

[21] A. Kylili, P. A. Fokaides, P. Christou, and S. A. Kalogirou, “Infrared thermography (IRT) applications for building diagnostics: A review,” *Applied Energy*, vol. 134, pp. 531–549, Dec. 2014, doi: 10.1016/j.apenergy.2014.08.005.

[22] ASTM E1933-14a, *Standard Practice for Measuring and Compensating for Emissivity Using Infrared Imaging Radiometers*. ASTM International, 2022.

[23] ISO 9869-1, *Thermal insulation — Building elements — In-situ measurement of thermal resistance and thermal transmittance — Part 1: Heat flow meter method*. International Organization for Standardization, 2014.

[24] ISO 6781, *Thermal insulation — Qualitative detection of thermal irregularities in building envelopes — Infrared method*. International Organization for Standardization, 2015.

[25] ISO 6946, *Building components and building elements — Thermal resistance and thermal transmittance — Calculation methods*. International Organization for Standardization, 2017.

[26] ISO 15099, *Thermal performance of windows, doors and shading devices — Detailed calculations*. International Organization for Standardization, 2003.

[27] National Fenestration Rating Council, Inc., *THERM 7 / WINDOW 7 NFRC Simulation Manual*. National Fenestration Rating Council, Inc., Jul. 2024.

[28] FLIR Systems, Inc., *FLIR C5 Datasheet*. FLIR Systems, Inc., Apr. 2020. [Online]. Available: https://www.flir.com/products/c5/. (Accessed: Feb. 19, 2025).

[29] FluxTeq, *FluxDAQ Ultra-High Resolution Heat Flux Sensor and Thermocouple Measurement System*. FluxTeq, n.d. [Online]. Available: https://www.fluxteq.com/heat-flux-thermocouple-data-reader. (Accessed: Feb. 19, 2025)

[30] FluxTeq, *PHFS-01 Heat Flux Sensor*. FluxTeq, n.d. [Online]. Available: https://www.fluxteq.com/phfs-01-heat-flux-sensor. (Accessed: Feb. 19, 2025).

[31] Onset Computer Corporation, *HOBO U12 Temp/RH/Light External Data Logger (U12-012) User's Manual (CE compliant)*. Onset Computer Corporation, 2016. [Online]. Available: https://www.onsetcomp.com/resources/documentation/13128-b-man-u12012-web. (Accessed: Feb. 19, 2025).

[32] 3M, *Scotch® Vinyl Electrical Tape Super 88 Data Sheet*. 3M, Jun. 2022. [Online]. Available: https://www.3m.com/3M/en_US/p/c/tapes/electrical/vinyl/. (Accessed: Feb. 19, 2025).

[33] Echotape, *MT-A7757 All Weather Aluminum Foil Tape*. Echotape, n.d. [Online]. Available: https://echotape.com/product-catalog/. (Accessed: Feb. 19, 2025).

[34] EDTM, *GC3200 GlassChek Elite*. EDTM, 2015. [Online]. Available: https://www.edtm.com/manufacturing-tools/manufacturing-glass-air-space-thickness-detector/gc3200-glass-chek-elite. (Accessed: Mar. 31, 2025).

[35] T. R. Geballe, "Atmospheric Transmission Data." Jun. 13, 2005. [Online]. Available: https://www.gemini.edu/sciops/instruments/mir/wavecal/N_ech.dat

[36] NASA, "Prediction of Worldwide Energy Resources (POWER) Project," NASA Langley Research Center. [Online]. Available: https://power.larc.nasa.gov/. Accessed: Mar. 23, 2025.

[37] M. Bosilovich, R. Cullather, and National Center for Atmospheric Research Staff (Eds.), "The Climate Data Guide: NASA's MERRA2 reanalysis," *The Climate Data Guide*, Jan. 19, 2024. [Online]. Available:

https://climatedataguide.ucar.edu/climate-data/merra2-modern-era-retrospective-analysis-research-and-applications. Accessed: Apr. 2, 2025.

[38] J. L. Wright, "A Correlation to Quantify Convective Heat Transfer Between Vertical Window Glazings," vol. 102.

[39] G. Ficco, F. Iannetta, E. Ianniello, F. R. d'Ambrosio Alfano, and M. Dell'Isola, "U-value in situ measurement for energy diagnosis of existing buildings," *Energy and Buildings*, vol. 104, pp. 108–121, Oct. 2015, doi: 10.1016/j.enbuild.2015.06.071.

[40] K. Zhang, T. P. McDowell, and M. Kummert, "Sky Temperature Estimation and Measurement for Longwave Radiation Calculation," presented at the 2017 Building Simulation Conference, Aug. 2017. doi: 10.26868/25222708.2017.569.